LEVEL

AD A088836

RESEARCH AND DEVELOPMENT TECHNICAL REPORT

2.06 MICRON-LASER RANGEFINDER TECHNOLOGY

FINAL REPORT
by
B.E. HENDRICKSON-L.S. O'HARA

SEPTEMBER 1979

DTIC
ELECTE
AUG 2 8 1980
S
C

ERADCOM

UNITED STATES ARMY ELECTRONICS RESEARCH
AND DEVELOPMENT COMMAND
NIGHT VISION AND ELECTRO OPTICS LABORATORY
FORT BELVOIR, VIRGINIA

CONTRACT DAAB07-77-C-2197

RCA | Government Systems Division
Automated Systems
Burlington, Massachusetts 01803

DDC FILE COPY

6

2.06 MICRON-LASER RANGEFINDER
TECHNOLOGY

9   FINAL REPORT.   *Sep 7' - Aug 79*

CONTRACT NO.   DAAB07-77-C-2197

15

Prepared by

10   B. E./Hendrickson ▬ L. S./O'Hara

RCA/Government Systems Division
Automated Systems,
Burlington, Massachusetts 01803

For

U. S. ARMY ELECTRONICS RESEARCH AND DEVELOPMENT COMMAND,
FORT BELVOIR, VIRGINIA

410699

DEPARTMENT OF THE ARMY
FORT MONMOUTH CONTRACTS OFFICE
U.S. ARMY ELECTRONICS RESEARCH AND DEVELOPMENT COMMAND
FORT MONMOUTH, NEW JERSEY 07703

DRDEL-AQ-M -2(KIN)   2 1 JAN 1990

RCA
P.O. Box 588
Burlington, MA 01803

Gentlemen:

The Draft Final Report submitted under CLIN 0006, Contract DAAB07-77-C-2197 has been reviewed and approved.

The only possible correction may be figure 3.3 on page 3-6. It is believed that this figure may originally have been developed by Sanders Associates of Nashua, NH. If this is the case, the source should be appropriately acknowledged.

DONALD A. FOSTER
MAJ, T/C
Contracting Office

RECEIVED

JAN 28 19

HC CENTER

REPORT DOCUMENTATION PAGE		READ INSTRUCTIONS BEFORE COMPLETING FORM
1. REPORT NUMBER	2. GOVT ACCESSION NO.	3. RECIPIENT'S CATALOG NUMBER
4. TITLE (and Subtitle) 2.06 Micron - Laser Rangefinder Technology		5. TYPE OF REPORT & PERIOD COVERED Final Report September 1978 - Aug. 1979
		6. PERFORMING ORG. REPORT NUMBER
7. AUTHOR(s) Bruce Hendrickson Larry O'Hara		8. CONTRACT OR GRANT NUMBER(s) DAAB07-77-C-2197
9. PERFORMING ORGANIZATION NAME AND ADDRESS RCA Corporation Automated Systems Burlington, Massachusetts		10. PROGRAM ELEMENT, PROJECT, TASK AREA & WORK UNIT NUMBERS
11. CONTROLLING OFFICE NAME AND ADDRESS Night Vision - Electro Optics Laboratory Fort Belvoir, Virginia		12. REPORT DATE September 1979
		13. NUMBER OF PAGES
14. MONITORING AGENCY NAME & ADDRESS(if different from Controlling Office)		15. SECURITY CLASS. (of this report) Unclassified
		15a. DECLASSIFICATION DOWNGRADING SCHEDULE

16. DISTRIBUTION STATEMENT (of this Report)

This document has been approved for public release and sale; its distribution is unlimited.

17. DISTRIBUTION STATEMENT (of the abstract entered in Block 20, if different from Report)

18. SUPPLEMENTARY NOTES

19. KEY WORDS (Continue on reverse side if necessary and identify by block number)

Laser Rangefinder	Rangefinder
HgCdTe	Detector
Holmium Laser	

20. ABSTRACT (Continue on reverse side if necessary and identify by block number)

A laser rangefinder receiver utilizing a photoconductive, thermoelectrically cooled HgCdTe detector was developed for detection of the 2.06 micron wavelength Holmium laser. The HgCdTe receiver was tested with an RCA developed Ho:YLF laser as a laser rangefinder. Quantitative ranging tests were conducted and compared to predicted results utilizing the measured Noise Equivalent Power (NEP) of $0.5 - 1.0 \times 10^{-11}$ watts/$\sqrt{Hz}$ of the detector pre-amplifier. A 1pps thermoelectrically cooled Ho:YLF laboratory laser was successfully developed and tested to $140°F$.

DD $_{1\ JAN\ 73}^{FORM}$ 1473   EDITION OF 1 NOV 65 IS OBSOLETE

TABLE OF CONTENTS

i

LIST OF ILLUSTRATIONS

LIST OF ILLUSTRATIONS (Cont'd)

LIST OF TABLES

I

INTRODUCTION AND SUMMARY

This program, conducted under contract DAAB07-77-C-2197, from September 1977 through August 1979 was directed at 1) development and test of a feasibility model laser rangefinder receiver operating at the 2.06 micron wavelength of the Holmium (Ho) laser in a laser rangefinder with a Ho:YLF laser and 2) development of a laboratory model thermoelectrically cooled Ho:YLF laser operating up to 1pps. This wavelength is attractive since the Holmium laser has greatly superior "eye safety" characteristics in comparison to Nd:YAG at 1.06 u. In addition the Holmium laser is reasonably efficient, compact and compatible with many components developed for Nd:YAG systems. Previous analysis (1) indicated that reasonable rangefinder performance using Ho:YLF lasers and HgCdTe detectors could be achieved, although there existed the possibility of severe atmospheric CO_2 absorption (2) which would limit performance.

The receiver was tested with an RCA developed Ho:YLF (Yttrium Lithium Fluoride) laser as a laser rangefinder (Figure 1-1) to determine, in actual ranging tests the capability of 2.06μm laser rangefinder. To the author's knowledge this is the first reported operation of a 2.06 micron laser rangefinder and demonstrated that atmospheric CO_2 absorption of 2.06 micron Ho:YLF laser radiation is not a significant factor in rangefinder applications.

The rangefinder receiver developed and described in Section II utilizes a thermo-electrically cooled, photoconductive HgCdTe detector. A special high frequency "boosted" pre-amplifier was utilized to extend the frequency response to 20 MHz for satisfactory detection of 50 nsec Q-switched laser pulses. A modified AN/GVS-5 Hand Held Laser Rangefinder video amplifier and a standard AN/GVS-5 range counter were utilized to determine and display in meters the range to targets. A 2.0 inch diameter lens and spectral filter were utilized to collect the received laser return signals. Quantitative ranging tests were performed and are reported in Section II. The results are compared to calculated performance based on measured detector and laser characteristics.

The laboratory model lpps Q-switched Ho:YLF laser is shown in Figure 1-2. This laser utilizes all conduction cooling of the Ho:YLF laser rod and flashlamp in conjunction with thermoelectrically cooling of the laser rod below ambient temperatures. This laser was operated at the program goal of lpps with 25% duty cycle operation (20 seconds on - 60 seconds off). Q-switching was performed with both $LiNbO_3$ Pockels Cell and rotating mirror. Operation up to $140^\circ F$ was achieved. Detail design and test data is contained in Section III.

This program has demonstrated its goals of showing the feasibility of a 2.06 micron laser rangefinder utilizing the Ho:YLF laser and HgCdTe detector in conjunction with standard laser rangefinder electronics of the AN/GVS-5. Reasonable rangefinder performance has been achieved including lpps operation in a simple compact configuration. It is concluded that this type laser rangefinder is entirely practical for many applications where the 2.06 micron wavelength is desireable. Further conclusions and recommendations are presented in Section IV.
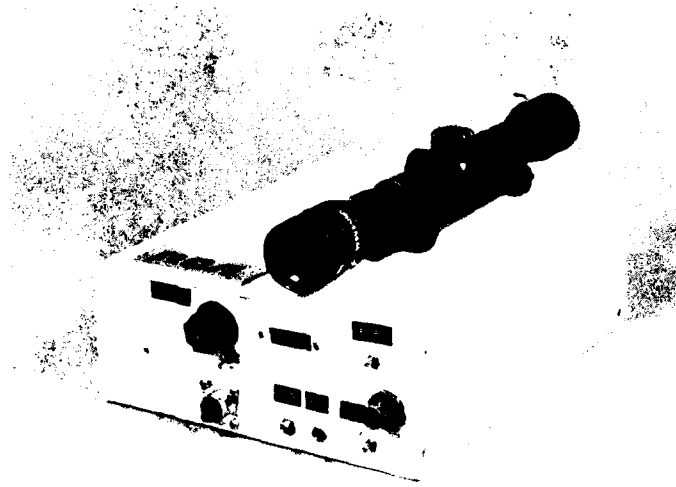
Figure 1-1. 2.06 Micron Ho:YLF/HgCdTe
Laser Rangefinder
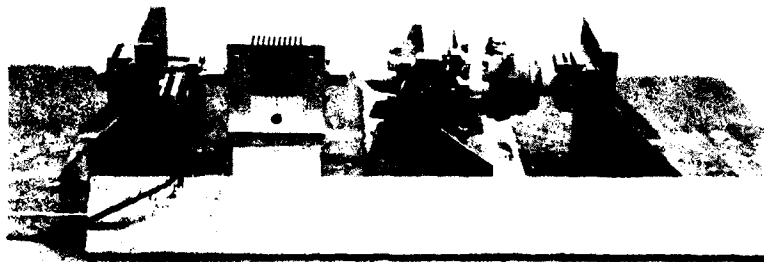
Figure 1-2. Laboratory Model 1 pps Ho:YLF Laser

Ho:YLF FEASIBILITY MODEL LASER RANGEFINDER

A. Description of the Rangefinder

The HgCdTe receiver described in this Section was operated with an RCA developed Ho:YLF laser as a rangefinder for the quantitative ranging tests described in this section. The Ho:YLF rod utilized Erbium and Thulium sensitizing ions and had a 0.35% Holmium concentration. The laser was Q-switched utilizing a rotating 100% flat mirror. Pulse widths were typically 40 - 50 nanoseconds although they could be as long as 150 nanoseconds. Q-switched energy outputs were 5-15 millijoules (depending on flashlamp and pump cavity conditions) into a 70% transmission telescope. It is noted that the laser was also operated with AN/GVS-5 power supply and trigger circuit further demonstrating the capability of a 2 micron laser rangefinder (LRF) to utilize components developed for Nd:YAG LRFs.

The laser and receiver were mounted to a common casting for boresight stability. Boresighting was accomplished with adjustment of the receiver optical axis. Aiming of the LRF was accomplished with a boresighted rifle scope.

B. Receiver Configuration

The 2.06 micron laser rangefinder receiver developed on this program utilizes a thermoelectrically cooled, photoconductive HgCdTe element with associated collection lens, filter, pre-amplifier, video amplifier and range counter to provide the range in meters from the time of flight of a Ho:YLF laser pulse to and from a remote target. The receiver configuration is shown schematically in Figure 2-1. Table 2-1 summarizes the receiver characteristics. Figure 2-2 shows the receiver section as finally mounted with the Ho:YLF laser.

1)   Detector/Pre-amplifier

The detector, mounted on a two stage thermoelectric cooler in a TO-3 package with a sapphire window, was procured from New England Research in Sudbury, Mass. The material utilized has a peak response at 3.7 micron as shown in Figure 2-3 and was utilized since good material with 2.1 micron peak response was not available. For more extensive discussion of detectors for 2.0 micron detection see References 3 and 4.

Responsivity of HgCdTe detectors varies as

$$R_\lambda (w) = \frac{k}{(1 + \omega^2 J^2)^{\frac{1}{2}}}$$

where J is the detector time constant and k is a function of the material parameters (3). Figure 2-4 shows the noise spectrum of the photoconductive HgCdTe detector utilized. It is apparent that the detector has a ~400 kHz roll off. Rangefinders typically require 10 - 20 MHz bandwidth for multiple target discrimination.

The decrease in R_λ with increasing ω is approximately 6 dB per octave. To yield a flat frequency response, the gain of the preamplifier following the detector was boosted at 6 dB per octave between 400 kHz and 10 MHz as shown in Figure 2-5. Total preamplifier bandwidth was 20 MHz.

Figure 2-6 shows the resultant noise spectrum of the detector/boosted preamplifier combination. Total rms noise measured at the preamp output using an RMS voltmeter with 20 MHz bandwidth was 1.1 mV. Load impedance of both the RMS voltmeter and spectrum analyzer measurements was 50 ohms. Impulse response of the detector/pre-amplifier combination was 30 - 40 nano-seconds. Measurements by the manufacturer indicated a D^* and NEP at 2.0 micron of 2×10^9 cmHz$^{\frac{1}{2}}$/ watt and 1.3×10^{-11} w/Hz$^{\frac{1}{2}}$ respectively.
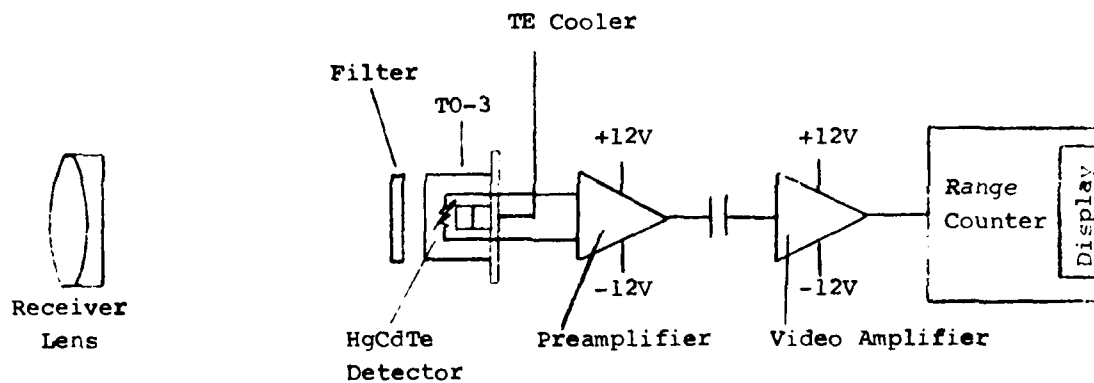
FIGURE 2-1. HgCdTe RECEIVER BLOCK DIAGRAM
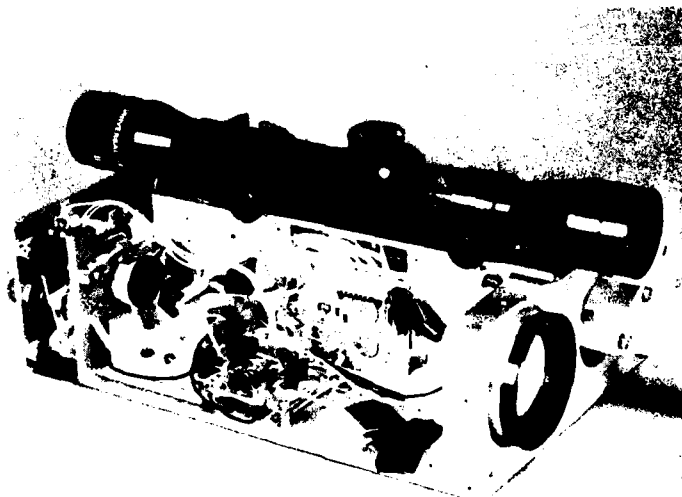
FIGURE 2-2. HgCdTe RANGEFINDER RECEIVER CONFIGURATION

TABLE 2-1.   2.06 Micron Receiver Characteristics

Detector Type:	HgCdTe, Thermoelectrically cooled
Wavelength, Peak Response, λ p:	3.7 microns
Detector Size:	0.010 x 0.010 inches square
Detector Temperature:	$\sim 230^{\circ}$K
Thermoelectrics:	Two stage, 1.0 amp, 1 Volt
Cool Down Time:	15-30 seconds
Bias Current, I_b:	0.4 milliamperes
Detector High Frequency Rolloff:	400 KHz
NEP (2.0 micron):	$0.5 - 1.3 \times 10^{-11}$ watts/Hz$^{\frac{1}{2}}$
D^* (2.0 micron):	$2-5 \times 10^{9}$ cm Hz$^{\frac{1}{2}}$/watt
Minimum Detectable Power:	$\sim 2 \times 10^{-7}$ watts at S/N = 7
Lens Aperture:	50mm Dia.
Filter Pass Band:	1.9 - 2.5 microns
Receiver Field of View:	1.3 x 1.3 milliradians square
Preamplifier:	Perry Model 3140-1 (Boosted Preamp 6 dB/octave above 400 KHz)
Overall Bandwidth:	0.5 - 20 MHz
Video Amplifier:	Modified AN/GVS-5
Range Counter:	Standard AN/GVS-5
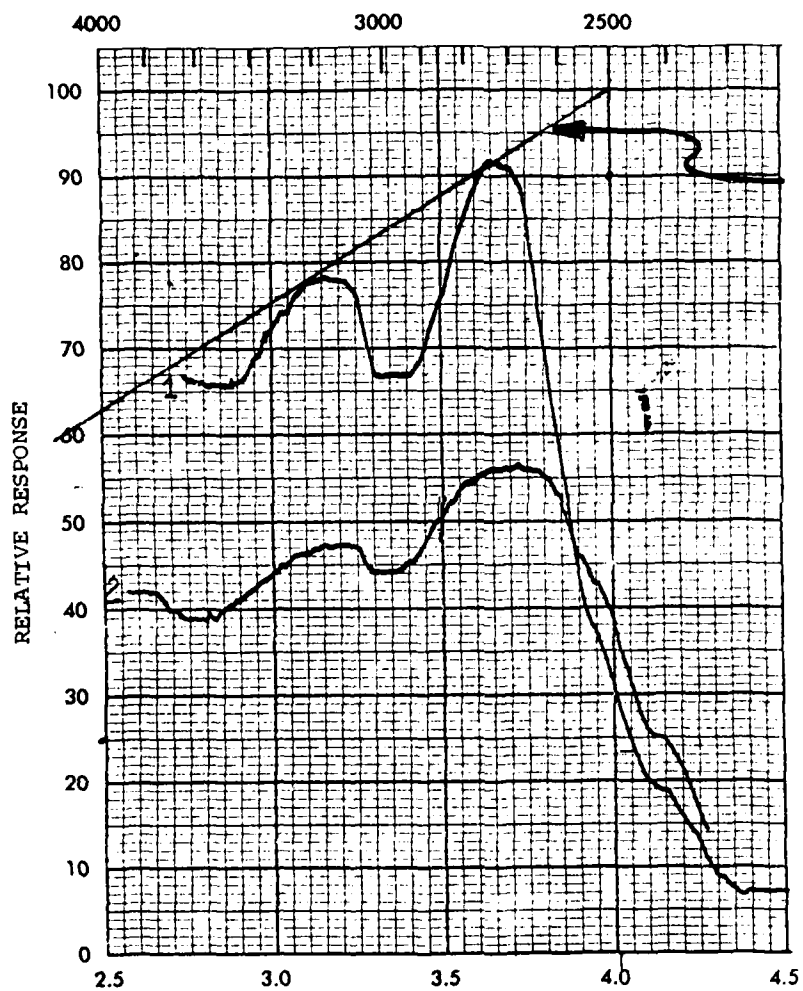
FIGURE 2-3. Responsivity vs. Wavelength for Photoconductive HgCdTe Detector Utilized in the 2 Micron Receiver (232°K)
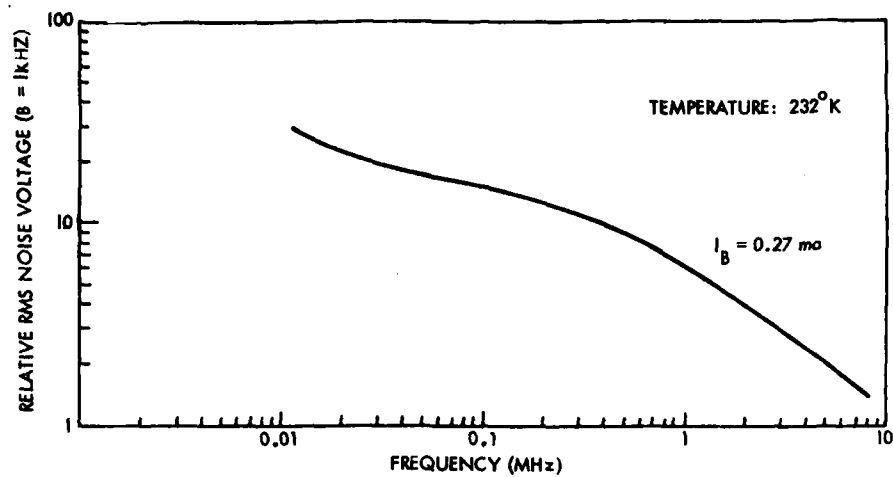
Figure 2-4. Noise Spectrum of the HgCdTe Detector
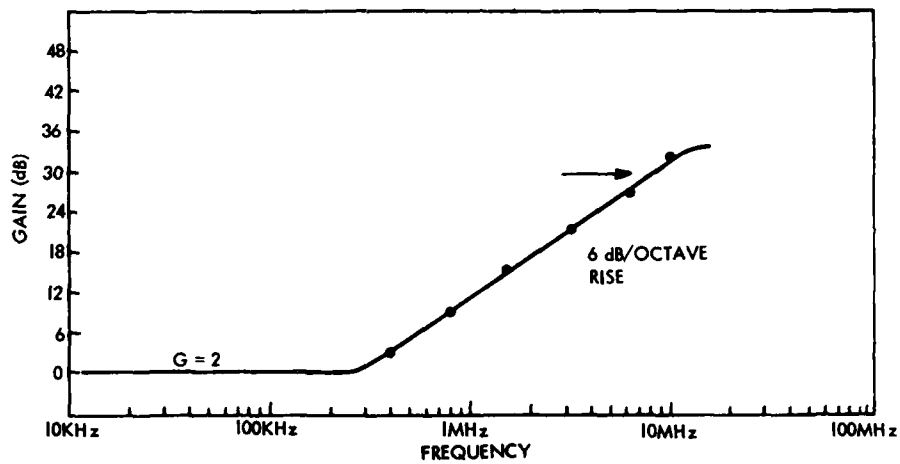
Figure 2-5. Frequency Response of Boosted Preamplifier
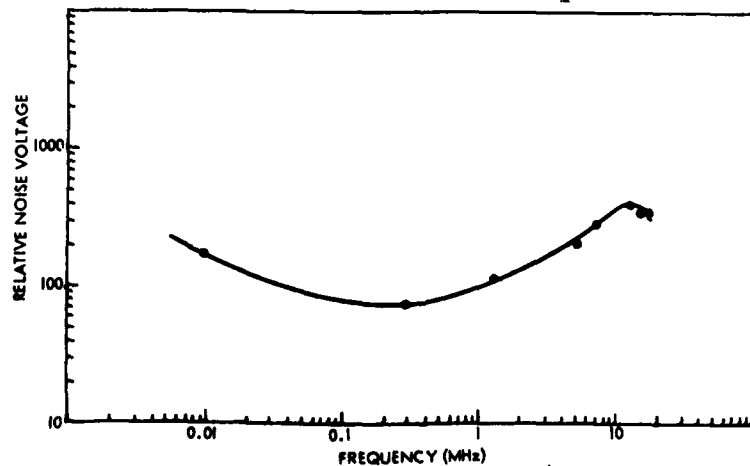
Figure 2-6. Noise Spectrum of HgCdTe Detector/Boosted Preamplifier

Further NEP - D^* measurements were performed on the HgCdTe detector/ preamplifier at 1.06 μ m utilizing a 6 nanosecond Nd:YAG laser pulse. With a peak power of 2.4 x 10^{-6} watts incident on the detector (at 230°K) a S/N of 13 was achieved with an output pulse width of 35 nanoseconds.

The equivalent NEP for the much wider $>$ 50 nanosecond, 2.06 micron pulses to be detected in the rangefinder was then calculated assuming a linear increase in responsivity with wavelength from 1.06 to 2.06 micron and a factor of 6 increase in amplitude response (and hence S/N) for the wider pulses for a 20 MHz noise bandwidth. The result is an NEP of 0.5 x 10^{-11} watts/Hz$^{\frac{1}{2}}$ and corresponding D^* of 5 x 10^9 cmHz$^{\frac{1}{2}}$/watt.

Following the detector preamplifier is a modified AN/GVS-5 Hand Held Laser Range-finder video amplifier. The video amplifier provides up to 37 dB gain over a 15 MHz bandwidth and performs threshold detection of received pulses. The pulses exceeding the threshold are passed to a digital counter to determine range. The AN/GVS-5 range counter was also employed in the 2μreceiver. Range measurements were displayed to an accuracy of $\pm$ 10 meters. Counter start was obtained by detecting laser output with an InAs detector.

2) Receiver Optics

The optical configuration of the receiver channel is shown in Figure 2-1. It consists of a cemented doublet achromat objective and a bandpass filter with the detector forming the field stop.

The objective is a standard 7 x 50 binocular achromatic objective with a visible focal length of 190 mm. Measured focal length at 2.06 microns is 197 mm. Measured transmission at 2.0 micron is 65%.

The filter is a 1.9 to 2.6 micron bandpass filter with 80% transmission at 2.06 micron. While somewhat wide in bandwidth, this filterwas chosen for its high

transmission at 2.06 micron in comparison to narrow band bilters. As shown below even this wide band filter is satisfactory since the background noise is negligible even with this bandwidth.

The worst case background power at the detector is given by:

$$P_B = \frac{\rho}{\pi} H_\lambda \alpha^2 A_r T_o B_o = 2.3 \times 10^{-7} \text{ watts}$$

where

P_B = background power at the detector (watts)

H_λ = solar irradiance at 2.06 micron $\dfrac{\text{watts}}{\text{cm}^2 - \text{nm}} = 7 \times 10^{-5}$

ρ = scene reflectivity = 1

α = angular field of view on a side of square FOV = 1.3×10^{-3} radians

A_r = Receiver objective area (cm^2) = 20

T_o = Optical transmission = .52

B_o = Optical passband (nm) = 600

The background generated noise current is $\sqrt{2e\beta P_B}$ = 2.5×10^{-13} amps/Hz$^{\frac{1}{2}}$ (assuming 50% quantum efficiency) in comparison to 4.2×10^{-12} amps/Hz$^{\frac{1}{2}}$ (NEP x β) for the detector.

Therefore, since the worst case background noise current is much less than the equivalent detector dark noise current the use of a 600 nm filter does not significantly effect overall detector sensitivity.

C. <u>Comparison of Calculated Ranging Capability with Ranging Test Data</u>

Using the range equation (1) an estimate of the maximum target range R, over which the rangefinder may be expected to operate was obtained.

$$(1) \qquad P_R = \rho \frac{T_o A_r P_t}{\pi R^2} \cdot e^{-2\sigma R}$$

where
P_R = Received Optical Power at the detector

ρ = target reflectivity

A_r = receiver lens area = 20 cm^2

P_t = peak transmitted power

R = target range (km)

R_V = visibility range (km)

σ = atmospheric attenuation coefficient at 2 um
for a given meterological visibility

The effects of atmospheric attenuation are included through the attenuation coefficient σ and range visibility R_V by assigning $2\sigma R_V = 3.5$. This is an intermediate value between 4.1 and 2.9 from references (1) and (6) respectively. Minimum detectable receiver power was determined from the NEP of the detector as shown below

$$P_{R\ MIN} = NEP \times \sqrt{B} \times \frac{S}{N}$$

where B is the preamplifier bandwidth and S/N is the required peak signal to rms noise ratio for a 99% probability of detection.

The required S/N ratio is 7. Substituting

$$P_R = 5 \times 10^{-12} \frac{W}{\sqrt{Hz}} \sqrt{20 \times 10^6 \ Hz} \times 7$$

$$= 1.6 \times 10^{-7} \text{ watts}$$

Energy through the laser telescope was typically 4 - 5 millijoules in a 40 nsec pulse (FWHM). This gives a transmitted power of 125 KW. Combined optical transmission of the receiver lens and interference filter was approximately 50% (T).

Employing equation (1) and the parameter values discussed above plots of R versus
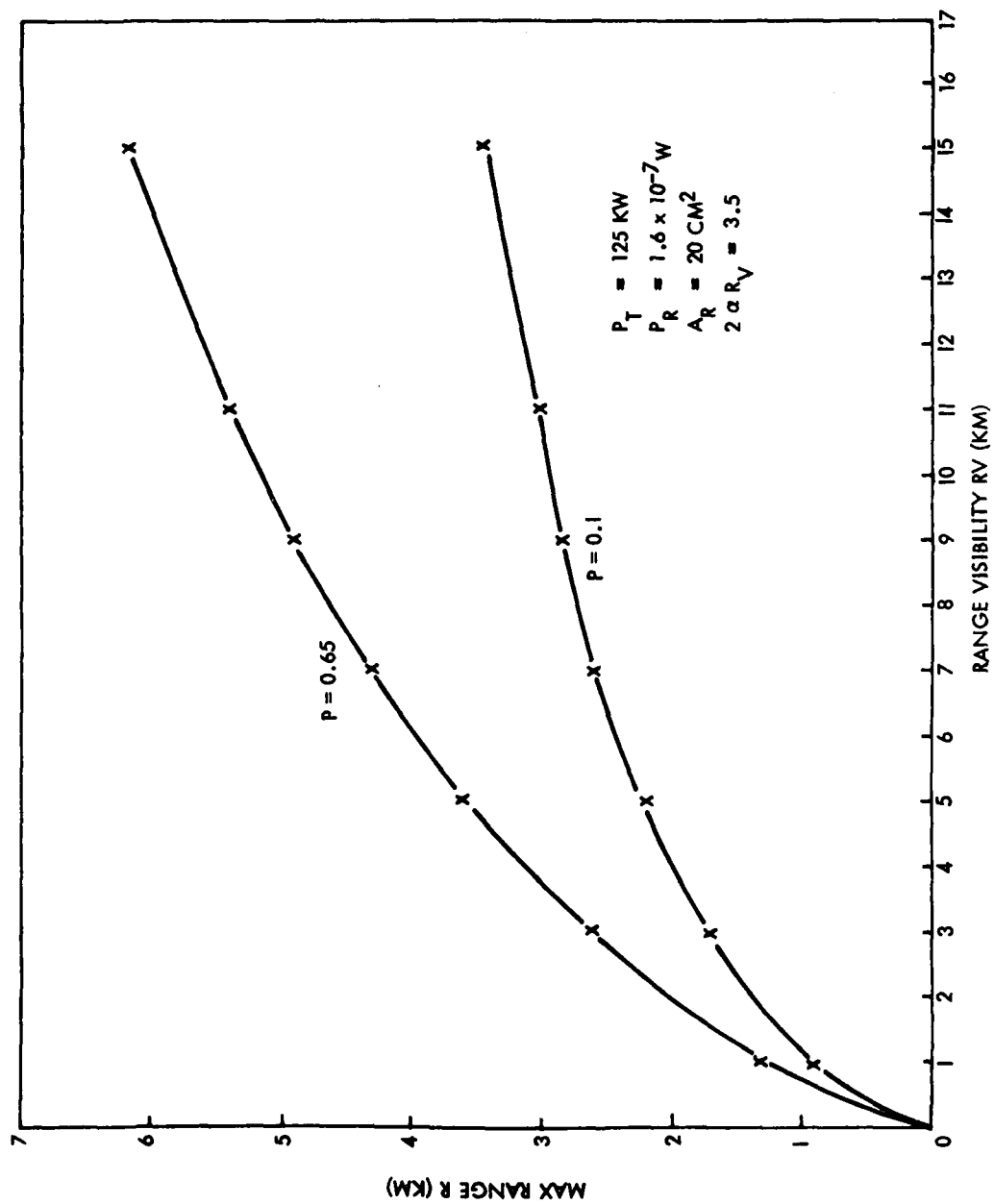
Figure 2-7. Calculated 2.06 Micron LRF Maximum Range Vs. Visibility Range

R_V for two values of target reflectivity (ρ, .1 and .65) have been made and are shown in Figure 2-7. Crossover points ($R=R_V$) vary from .65 to 1.5 km.

Targets available for testing the unit were a watertower at 1750 meters and a tree-line at 1100 meters. The water tower was painted a light green. Reflectivity of the tower at 2μ was estimated to be 65%. Reflectance of the treeline was estimated at 10% as shown in Figure 2-8 and 2-9.

The rangefinder was field tested on the two targets under varying atmospheric conditions. A summary of the extreme conditions is shown in Table 2-2. Performance of the rangefinder was evaluated by placing an iris at the receiver lens and stopping down (reducing A_R) the aperture until further reduction resulted in no returns.

TABLE 2-2

TOWER TARGET (1750 meters)

Range Visibility R_V	Min. Aperture Diameter	Calculated Range Capability
3.2 km (in light rain)	.6 in	1500 m
12.8 km	.3 in	1500 m

TREE LINE TARGET (1100 meters)

Range Visibility	Min. Aperture Diameter	Calculated Range Capability
3.2 km (in light rain)	.7 in	900 m
12.8 km	.4 in	

Using the receiver area A_R calculated from the iris opening and the appropriate target reflectivity (ρ=.65 or .1) equation (1) was solved for R, the maximum range capability we might expect of the rangefinder with the given A_R and atmospheric conditions. In general, the unit performed 15% better than might be expected.

The fade margin, i.e., the ratio of minimum receiver area for ranging to maximum aperture, was 10.5 dB (R_V = 3.2 km light rain) to 16.5 dB (R_V = 12.8 km) against the tower and 9 dB against the treeline in light rain.
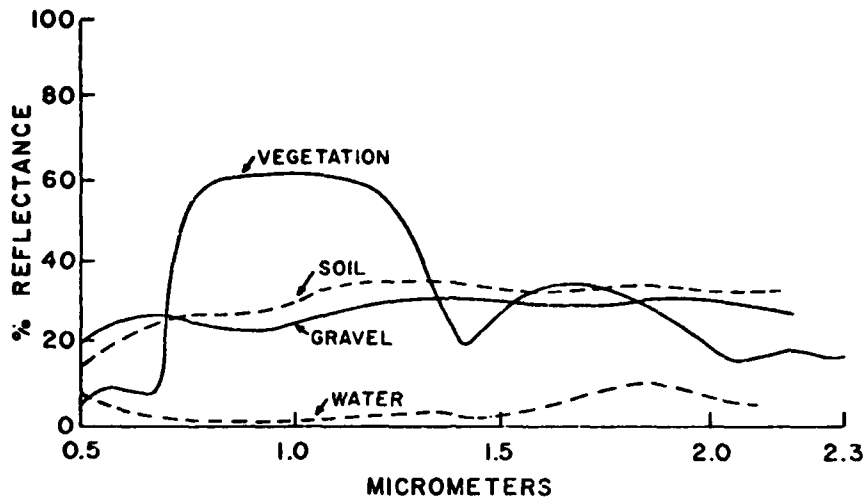
D-192

FIGURE 2-8   Reflectance of Some Natural Objects (1,5)
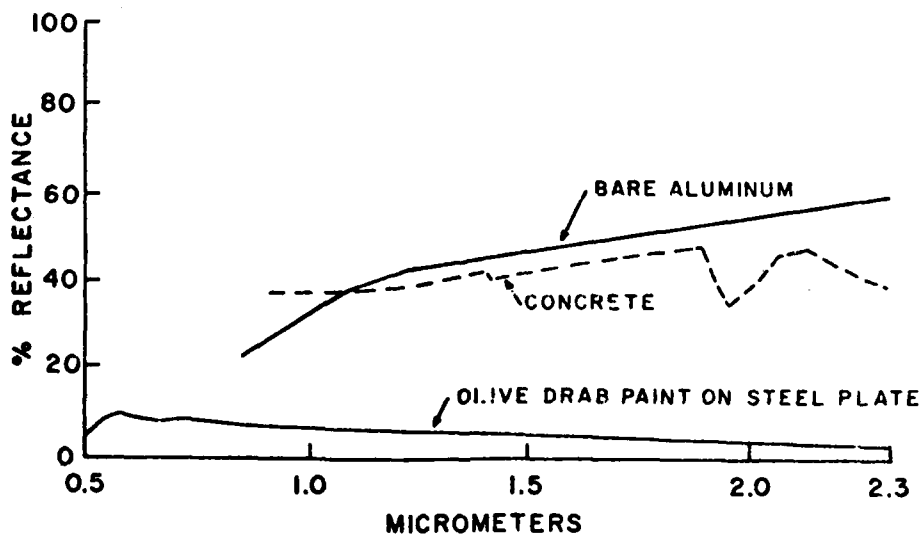
D-191

FIGURE 2-9.   Reflectance of Some Man-Made Objects (1,5)

2-13

III

1 PPS Ho:YLF THERMOELECTRICALLY

COOLED LASER

A. Development Objectives

The development objectives for the miniature 2.06 micron laser are summarized in
Table 3-1 together with the results achieved on this program for $LiNbO_3$ Pockels
Cell Q-switching and a separate RCA program which utilized a rotating mirror
Q-switch. The performance objectives are typical of many requirements found
in laser rangefinder applications.

Time limitations did not permit complete testing and optimization of the
$LiNbO_3$ Pockels Cell Q-switch. However, sufficient successful test results
with this Q-switching approach, together with the results of the rotating mirror
Q-switch, have been obtained. This effort has, therefore, demonstrated reliable
operation of the Ho:YLF laser suitable for use in military environments for
1 pps small laser rangefinders with the program objectives essentially demonstrated.
While further engineering development is indicated the basic performance
capabilities have been shown.

This section presents the detail design characteristics and test results
achieved. Areas of difficulty are noted and those areas requiring further
engineering indicated, e.g. programmable PFN energy control for transient duty
cycle operation under varying ambient temperature conditions.

Table 3-1. Ho:YLF Laser Module Performance

	Objective	LiNbO$_3$ Pockels Cell	RCA Rotating Minor
Mode of Operation	Single Pulse Q-switch	Single Q-switch	Single Q-switch
Energy/Pulse	10mJ	10mJ	10-40mJ
Pulse Width	40 nsec	150 nsec	55 nsec
Beam Divergence	6 mr, 80% Energy	2.6 mr	3.7 mr
Repetition Rate	1 pps	1 pps	1 pps
Duty Cycle	20 sec on,60 sec off	10 sec on, 60 sec off[+]	20 sec on, 60 off[*]
Stored Energy/Pulse	20 Joules	24 Joules[+]	25-35 Joules[+]
Additional Power	10w/pulse/sec	3 watts[+]	8 watts[*]
Ambient Temperature	-40°F to 145°F	to 140°F[+]	to 140°F[*]
Size	6x2x2 inches	9x2x2 inches	6.5x2x2

[+] Single ended TE cooled, constant 24J Input, tested only at room temperature, extrapolation to 145°F based on expected similarity to rotating minor performance.

[*] Dynamic Increase in pump energy. Tested to 145°F Ambient.

B. DESIGN CONSIDERATIONS AND DESCRIPTION

The Ho:YLF laser design developed is shown in Figure 3-1. A schematic cross-section of the pump cavity and resonator is shown in Figure 3-2. The two primary areas of laser design were the pump cavity/rod cooling and $LiNbO_3$ Pockels Cell Q-switch. The laser rod is cooled below ambient by a two-stage thermoelectric cooler while flashlamp/pump cavity is conduction cooled to the mounting baseplate. The $LiNbO_3$ Q-switch in conjunction with a ZnSe Brewster angle polarizer is square wave switched to generate a single Q-switch pulse.

These two design features of this Ho:YLF laser were implemented due to the characteristics of the Ho:YLF laser. An energy level diagram of $\alpha\beta$ Ho:YLF utilizing Erbium and Thulium sensitizers is shown in Figure 3-3. Ho:YLF is a quasi-three level laser at room temperature due to significant thermal population of the terminal laser level and exhibits $\sim$ .3 Joule/$^\circ$C temperature variation of threshold (7). The Erbium and Thulium sensitizers resonately transfer energy to the Ho:YLF metastable level (7).

Figure 3-4 shows the excitation spectrum of a Ho:YLF laser rod. It should be noted that the composition of the rod used for the present work is $LiY_{.429}Er_{.5}Tm_{.067}Ho_{.0034}$ grown by Sanders Associates (7). The relative pump efficiency of the various pump bands of Ho:YLF are shown in Table I below (7).

TABLE 3-2

Pump Band Efficiencies (7)

Wavelength (um)	Relative Excitation Efficiency
.28 - 2 um	100%
.28 - .57 um	67%
.57 - 2 um	33%
.40 - 2 um	80%
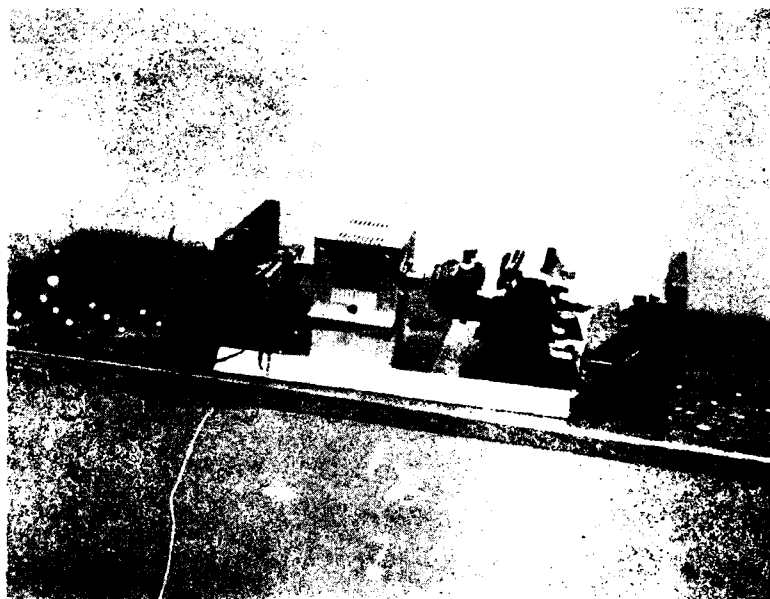
FIGURE 3-1.   1 pps Ho:YLF LASER
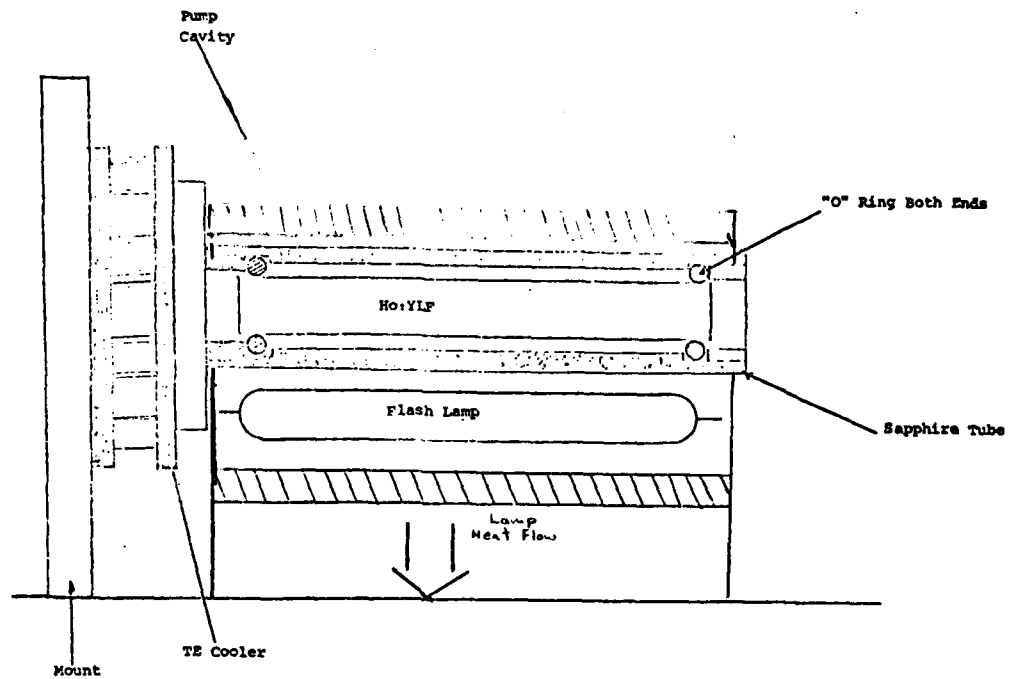
Thermoelectrically Cooled Ho:YLF
Pump Cavity Approach
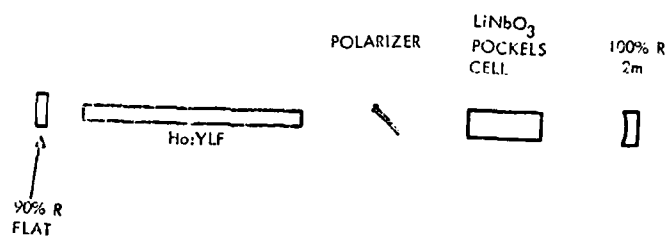
Ho:YLF pockels cell resonator.

FIGURE 3-2. 1 pps Ho:YLF LASER MODULE APPROACH
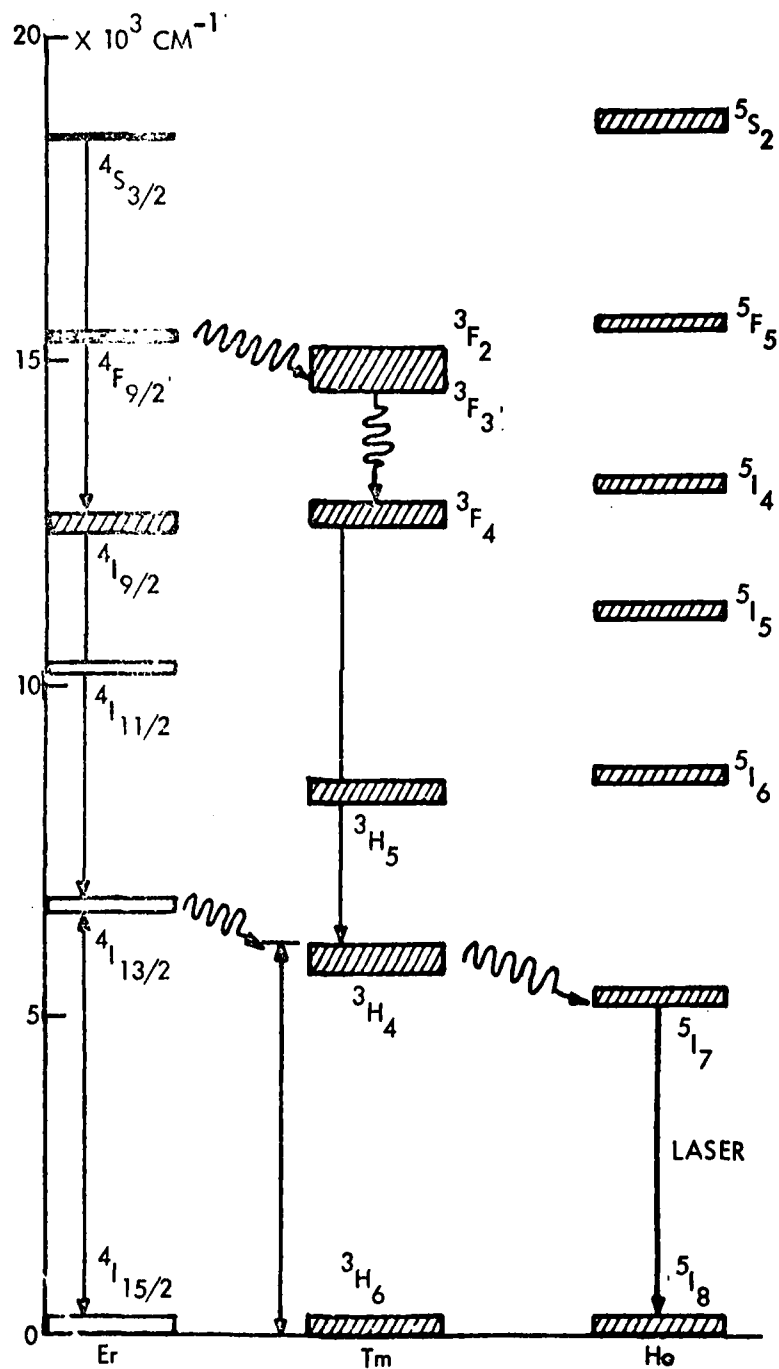
FIGURE 3-3.   LEVELS OF Er, Tm, Ho (7)

SAMPLE # 342

LiY$_{0.416}$Er$_{0.5}$Tm$_{0.067}$Ho$_{0.017}$

2 μM FLUORESC AMPLITUDE

PUMP WAVELENGTH (μm)

0.2 0.4 0.6 0.8 1.0 1.2 1.4 1.6

D-183
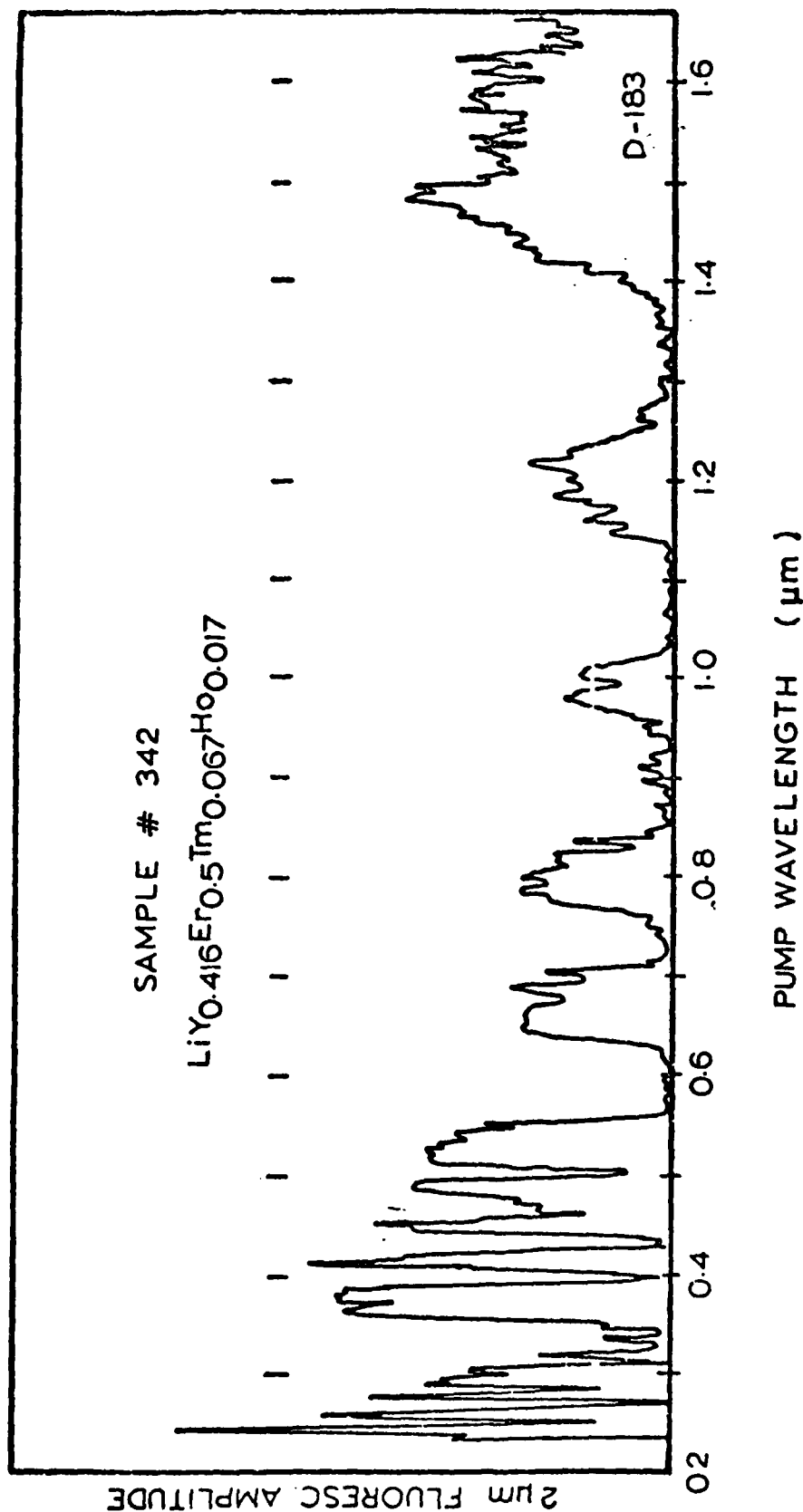
FIGURE3-4 EXCITATION SPECTRUM OF α/β -YLF

Amplitude Information should not be inferred from this drawing

•Lowel Noble, ILC Corp.

It can be seen that the most efficient pump band occurs in the .28 - .57 um region though significant pumping occurs as far out as 2 um.

The transfer time from the Erbium and Thulium to Holmium is slow-microseconds (7). This results in a great susceptibility to multiple pulsing when conventional step switched Pockels cell Q-switched except just above threshold where energy output is low. The multiple pulse behavior is aggravated by piezo-electric ring in LiNbO$_3$ Q-switches (7,8) typically used with Ho:YLF due to good transmission at 2.06 micron.

The above laser and Q-switching characteristics led to the design approach described in this section of a thermoelectrically cooled Ho:YLF rod to keep the rod cooled to near room temperature for 1 pps operation at elevated ambient temperatures. To suppress multiple pulsing which would lead to erroneous range in a rangefinder a square wave Q-switch drive for the LiNbO$_3$ was utilized.

1) PUMP CAVITY AND ROD COOLING DESIGN PERFORMANCE SUMMARY

The pump cavity and thermoelectric (TE) rod cooling design are shown in Figure 3-2. The pump cavity is air filled. The heat absorbed by and conducted to the cavity walls from the quartz envelope flashlamp is conducted to the ambient temperature base plate heat sink through the aluminum cavity housing structure.

The selected method of cooling a 1 pps Ho:YLF laser rod employs conduction heat sinking with thermoelectric (TE) cooling. TE technology is well developed, has minimal space requirements, and in itself does not effect pump efficiency. TE's permit cooling below ambient to any level consistent with power considerations. This reduces the laser threshold and heat dissipation in the laser rod and flash-lamp.

The rod is separately heat sunk by a "cladding" sapphire tube with a thin film of liquid in the annulus between the laser rod and cladding tube. The heat generated within laser rod is conducted into the sapphire and conducted down the tube to the

thermoelectric (TE) cooler which is mounted on a separate heat sink support from the pump cavity. This minimizes the heat load to the TE cold side. The heat load which must be cooled by the TE is the combination of Ho:YLF generated heat and ambient heat picked up by the cold sapphire finger in the warm cavity air. This type of single ended heat sinking results in an axial temperature gradient in the rod.

A summary of the calculated thermal and operating design point character istics of the detail design described in the following sections is presented in Table 3-3. If the rod was not TE cooled below ambient an additional 10-20 joule/pulse lamp input would be required due to the threshold increase of Ho:YLF with temperature. TE cooling then appears to offer significant advantages for a 1 pps repetition rate.

TABLE 3-3. SUMMARY ESTIMATED DESIGN POINT CHARACTERISTICS

Ambient Temperature - 145°F

Internal Cavity Air Temperature - 250°F

Thermoelectric Cold Side Temperature - 32°F

Rod Thermal Generation Rate at 1 pps - 0.5 watts

Convective Heat Load to TE - 1.2 watts

Average TE Heat Load - 1.3 watts

Average Laser Rod Temperature - 86°F

Flashlamp Energy per Pulse - 20 Joules

TE Input Power - 6 watts max

2) ROD CONDUCTION COOLING DETAIL DESIGN

Thermoelectric conduction cooling of the 3 x 30 mm cylindrical Ho:YLF laser rod is accomplished by placing the rod in a sapphire tube 46mm x 6mm OD x 3.2mm ID (see Figure 3-5). The sapphire tube is countersunk at each end to a depth of 10mm and an ID of 4.2mm. The rod is centered longitudinally within the tube and supported by 70 durometer silicone O-rings at each end. Silicone was selected
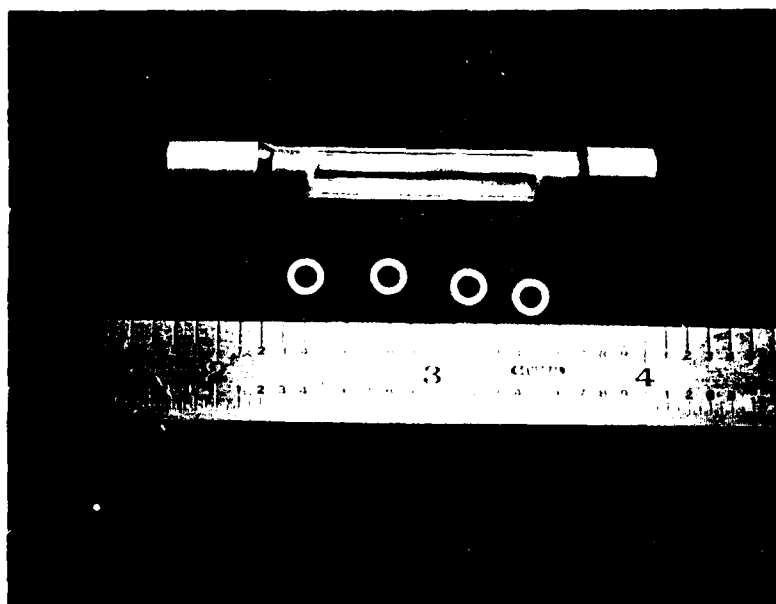
FIGURE — . —— — — — — — — — — — — — — — — — TUBE

because of its compatibility with ethylene glycol and resistance to ultra-violet radiation. The O-rings are seated against the countersink step by beryllium-copper sleeves and lock rings as shown in Figure 3-6. Thermal contact with the laser rod is maintained by filling the gap between the O-rings with a suitable optically transparent, thermally conductive medium (ethylene glycol and water (EGW) being used in the unit). The entire rod, tube, and coolant assembly threads to a beryllium-copper interface spacer in good thermal contact with the cold side of the TE cooler as shown in Figure 3-7.

The thermal conductivity of sapphire is approximately seven times that of YLF (.47 vs. .063 watts/cm$^{\circ}$C). Heat generated within the rod is conducted radially through the nominal .1mm coolant gap to the sapphire tube, then longitudinally down the tube through the BeCu interface spacer to the TE cooler. One or two flashlamps are positioned parallel to the tube. The flashlamps and pump cavity assembly are supported independently of the rod and tube to eliminate conduction heat loading of the rod and provide easy access. Convective and radiative loading of the rod are still significant, however, particularly at the increased internal ambients present during operation.

3) PUMP CAVITY AND FLASHLAMPS

The experimental pump cavity (Figure 3-8) is fabricated of aluminum and is base mounted separately from the sapphire tube and TE cooler. It is designed to accept a variety of pump geometry inserts. This allows for easy inspection of the sapphire tube, o-rings, and laser rod during the course of testing without disturbing the resonator alignment. Inner cavity surfaces are coated with vacuum deposited aluminum to insure high reflectivity (R > 90% at .25um) in the Ho:YLF pump bands. Previous experience with Ho:YLF has indicated good pumping characteristics are obtained with close wrap cavities. Single flashlamp and dual flashlamp close wrap cavity inserts can be accomodated. A dual flashlamp cavity offers the advantage of a balanced thermal input to the rod while single flashlamp cavities have higher pumping efficiency.

3-11

FIGURE 3-6. 4-PIN SEAL AND THERMALLY
NONCONDUCTIVE SUBSTRATE TO BE USED

2 Stage TE Cooler

T.E Cooler Hot Side Sink

Thermally Insulating Standoff

Interface Spacer

Sapphire Tube

TE Cooler Cold Side Plate
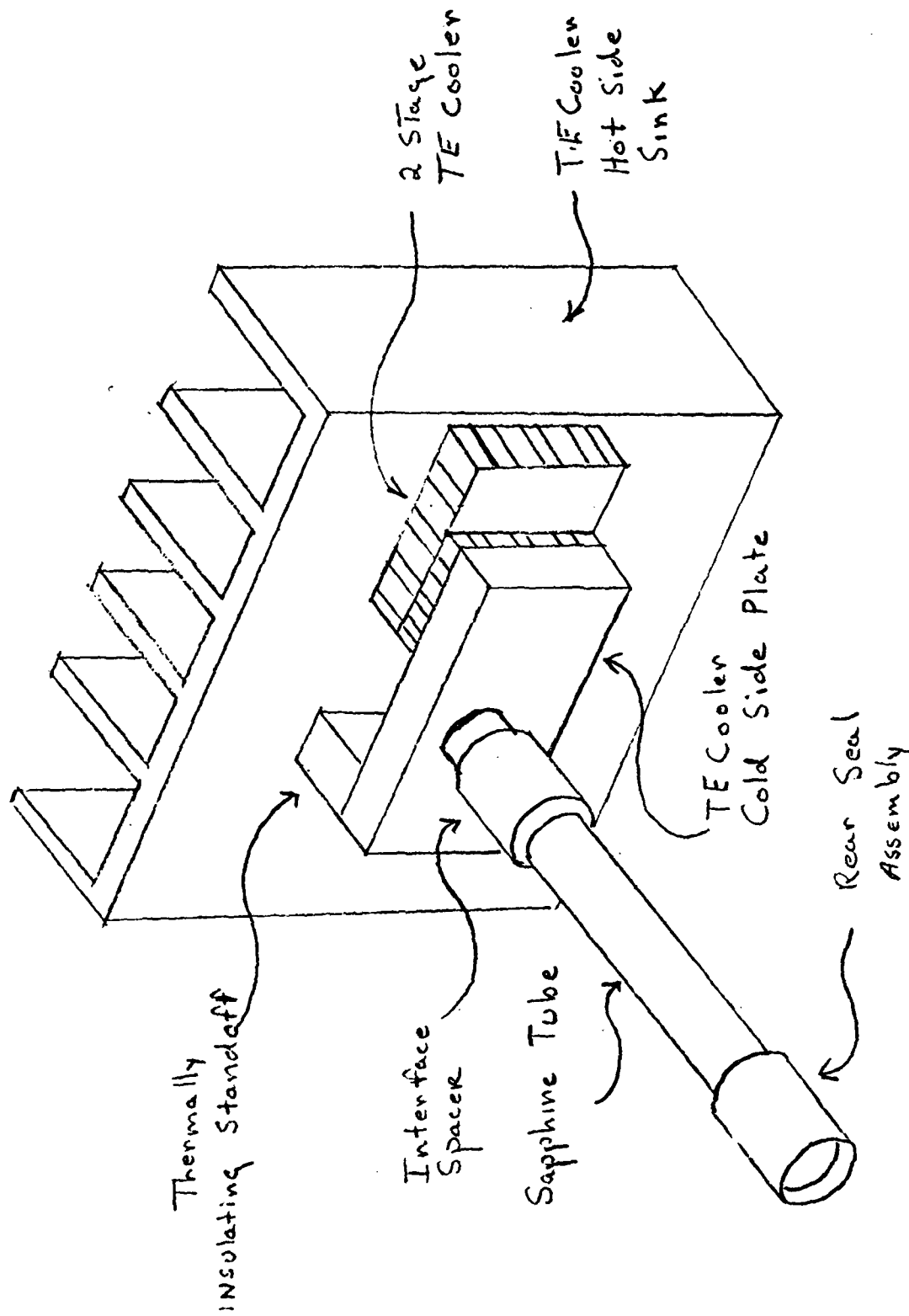
Rear Seal Assembly
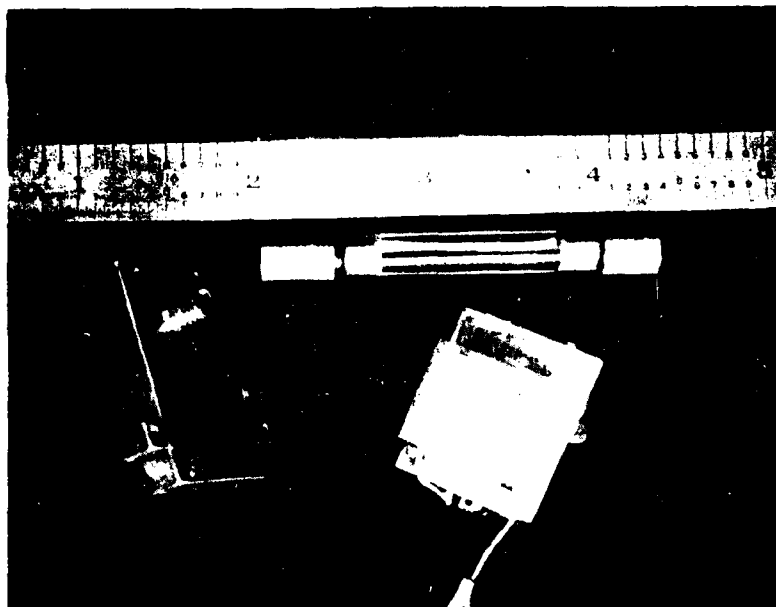
FIGURE 3-7. MOUNTING OF SAPPHIRE TUBE AND
LASER ROD TO TE COOLER AND ARBITRARY HEAT SINK

Note the pump cavity and flashlamps normally enclosing the tube are not shown

FIGURE 3-8. PHOTOGRAPH SHOWING PUMP CAVITY AND
FLASHLAMP MOUNTING (SINGLE FLASHLAMP CAVITY)

External dimensions are the same for both cavities. Only the internal configuration need be modified to accomodate the second flashlamp if desired. Electrical insulation of the flashlamp electrodes is provided by ceramic end caps potted to the electrodes.

The 29mm arc length quartz envelope xenon flashlamps (EGG XFXQ-34-1.1) are supported by the pump cavity so that some conduction cooling of the lamps is possible. The envelope material is quartz to provide maximum transmission in the Ho:YLF pump bands. Preliminary work at specifying optimum flashlamp characteristics for Holmium lasers has been performed by Noble, et al (9). Based on this work bore diameter of the lamps was specified as 3mm and the nominal optical pulse width as 200 usec. Noble et al (10) have also determined that fill pressures near 3000 torr provide the most output in Ho:YLF pump bands. The XFXQ34-1.1 flashlamps possess a lower fill pressure of 700 torr. These were selected based on more reliable triggering at the lower pressure, availability and dimensional requirements.

4) Q-SWITCHED OUTPUT OF Ho:YLF

Reasonable rangefinder performance will require a Q-switched laser module. Saturable dye Q-switches are not currently available at the 2.06um wavelength of the Ho:YLF laser. Therefore, a Pockels Cell or other type Q-switch will be required. Significant difficulty exists in obtaining reliable single pulse Q-switched operation of Ho:YLF using $LiNbO_3$. Hilberg and Hook (8) have found that although voltage across the $LiNbO_3$ decreases to zero during switching, a residual retardation persists. This results in reduced transmission through the Pockels Cell Q-switch and high intracavity losses when switched from the $\lambda/4$ wave voltage to ground. In addition, $LiNbO_3$ suffers from piezoelectric ringing whose severity is a function of electrode contact materials and pressure. The ringing allows significant numbers of afterpulses in Q-switched operation.

3-15

The residual retardation losses after switching can be somewhat reduced by maintaining a compensating electrical potential across the crystal after switching. After-pulsing can be suppressed by returning the potential to the $\lambda/4$ hold-off voltage provided piezoelectric ring does not significantly modulate the $\lambda/4$ retardation. Common to any Pockels Cell Q-switch is a polarizer. A ZnSe single plate Brewster polarizer was selected over a Glan-Air calcite due to superior transmission which should enhance efficiency. ZnSe also has a high index of refraction ($r = 2.45$) making it ideal for a Brewster polarizer.

Therefore the ideal voltage waveform is that shown in Figure 3-9. The circuit shown in Figure 3-10 was developed to achieve this effective waveform. In operation the crystal is biased to the $\lambda/4$ wave voltage by applying the $\lambda/4$ wave voltage from V_{BB} to one electrode. The ground electrode is pulsed to a higher voltage V_{CC}. The differential voltage being the desired compensating voltage after which it returns to ground potential thereby restoring resonator hold-off.

C_2 is an AC bypass of the power supply V_{BB}. C_1 is initially charged by the HV supply to a voltage (V_{CC}) slightly greater than V_{BB}. A five to six volt trigger pulse is then applied to the circuit causing V1 to conduct. This nominally places the charging voltage V_{CC} at C1 across the Pockels Cell giving the cell a net negative bias for the duration of the HV pulse. The high voltage pulse width is determined by the length of time required to build sufficient voltage on the grid of V2 to cause conduction to ground. The grid time constant is governed by the choice of R1 and C4. The rise and fall time of the high voltage pulse is set by R2 and C3. Rise times of 20-30ns are obtainable.

The resultant transmission characteristics of the LiNbO$_3$ probed with a HeNe laser using the square wave switch is shown in Figure 3-11. The extent of the remaining piezoelectric ringing in LiNbO$_3$ is evident. Without very careful electrode contacting the ring is significantly worse than that shown in the figure. This figure shows the modulation characteristics of a LiNbO$_3$ crystal placed between crossed polarizers and probed by a collimated HeNe laser. A 3.2kV square wave (500ns rise and fall time) was switched across one crystal electrode while the other was maintained at 3.3kV.
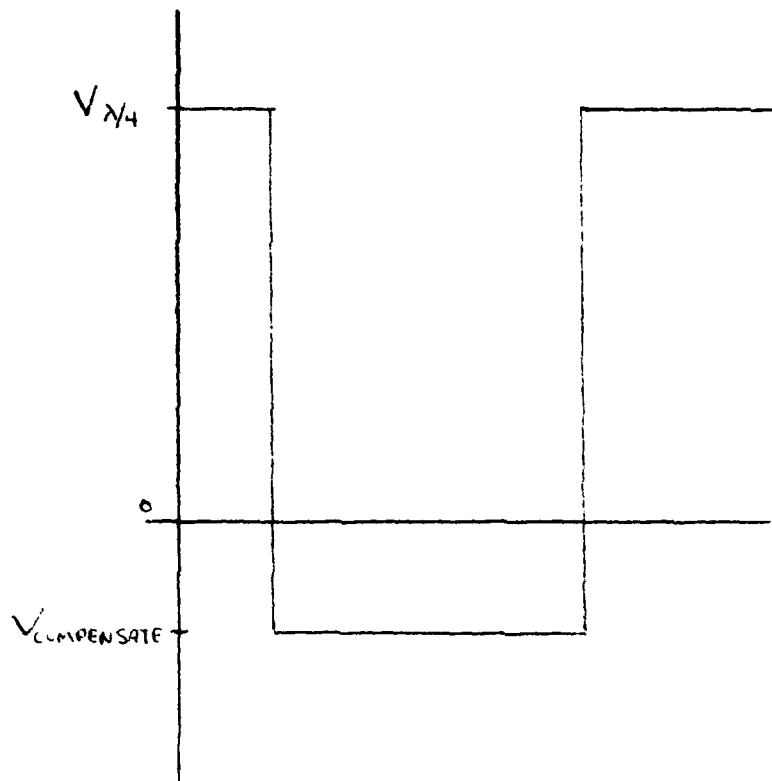
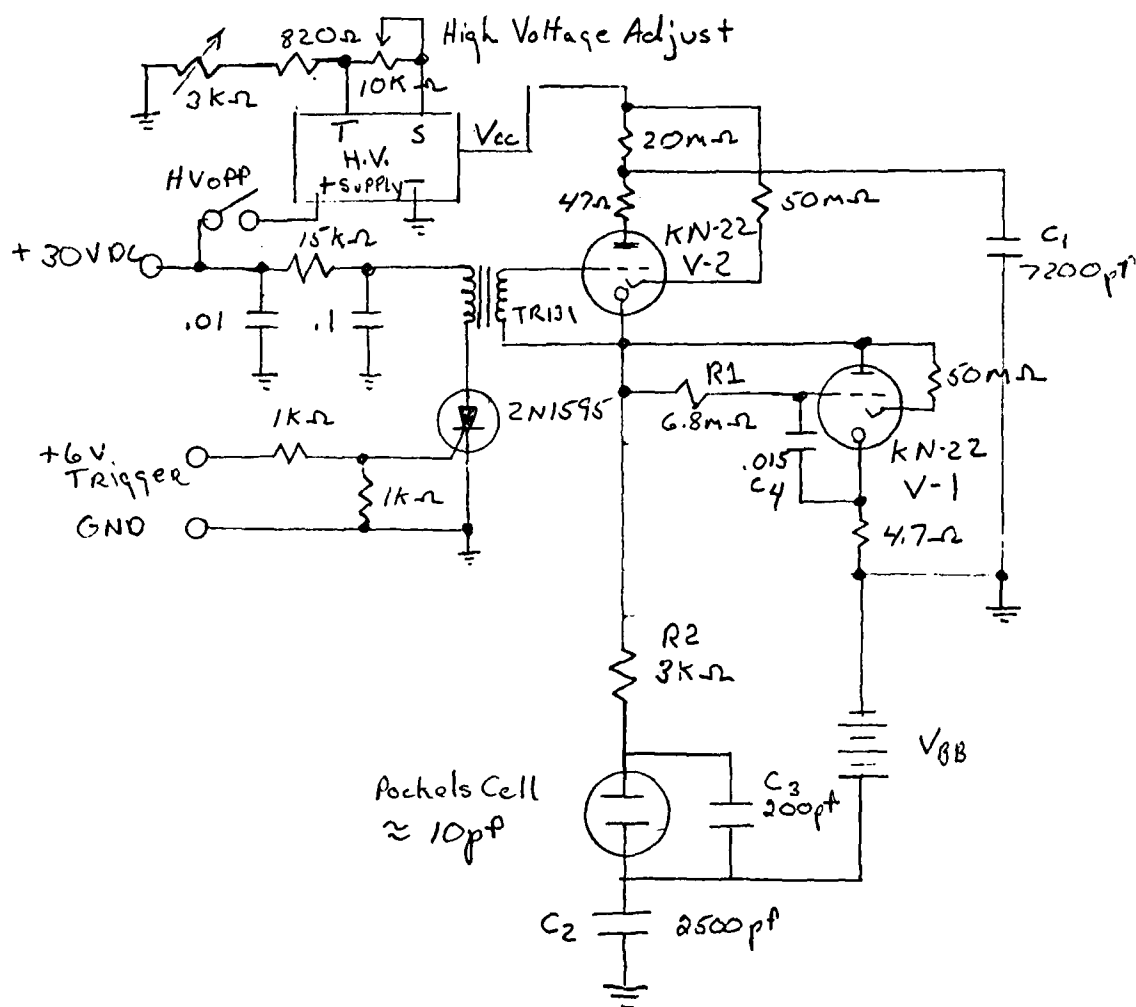FIGURE 3-9. IDEAL LiNbO$_3$ SWITCHING POTENTIAL

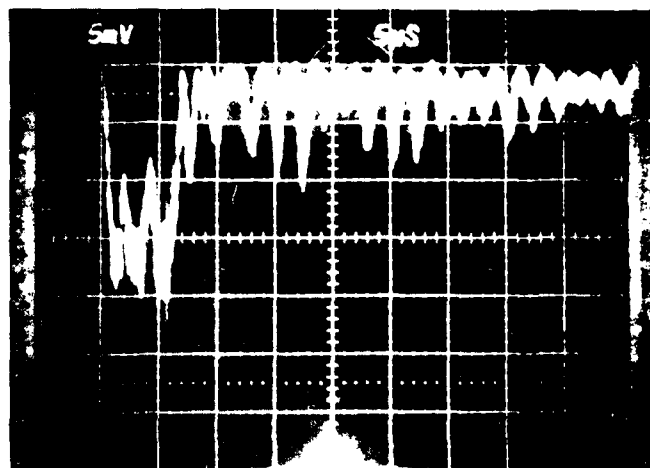FIGURE 3-10. SQUARE WAVE POCKELS CELL SWITCHING CIRCUIT

FIGURE 3-11. PIEZOELECTRIC RINGING IN LEAD, AT 2.5 MHz

C.   LASER OPERATION

Long pulse laser operation was first obtained using the laser resonator
shown in **Figure 3-1** less the Pockel's Cell.   To allow easier access to the
experimental setup the output mirror shown to the left was removed from
the TE heat sink to a separate mounting plate.   This resulted in an overall
resonator length of approximately 9 inches - slightly longer than that in-
dicated in the photograph.

1)   Long Pulse Operation

Figure 3-12 shows a photograph of the long pulse laser output detected by a
Judson Infrared J-12-LD InAs detector   ($\approx$ 10 ns).   Onset of the laser
output was   250 usec after the flashlamp trigger pulse and continued
until 600-700 usec after the trigger.   The output shown was obtained using
a close wrap pump cavity and 95% (R =∞) and MAX R (1 meter) reflectors.

Table 3-3 below shows the measured threshold for various resonator conditions.
Testing was expedited by operating the TE cooler at a low input level (.5A)
and pulsing the laser at 3-4 ppm.   This condition maintained the rod near
room temperature conditions.

TABLE 3-4   Long Pulse Thresholds

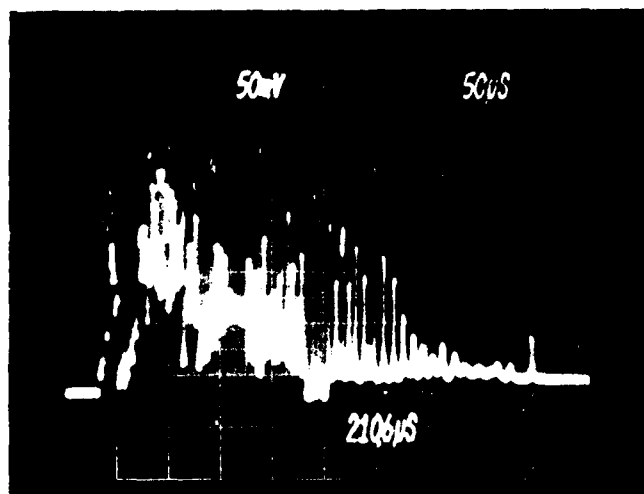| M1 M2	Resonator	Threshold
95% (∞) MAXR (1 meter)	Bare	18 joules
85% (∞) "	Bare	19.5 joules
85% (∞) "	Plus LiNbO$_3$	21.5 joules
85% (∞) "	Plus LiNbO$_3$ and Zn Se	21.5 joules

Figure 3-12

Long Pulse Output of Laser Resonator
containing Pockel's cell (85% flat, MAXR
1 meter). Quartz lamp pumped at 23 joules.
(50mV/div, 50 usec/div, scope delay 210 usecs).

Threshold for the bare resonator is 1.5-2.5 joules higher than those previously achieved using a quartz tube and RTV O-rings. This can, in part, be explained by the present rod mount in which 4-5 mm of the 30 mm rod is shaded by the O-rings and sleeves, the higher Fresnel losses of sapphire compared with quartz, and any absorption by the EGW mixture.

To obtain some idea of the unit's rep rate capabilities with a minimum of variables the laser was operated long pulse at 1pps, 20 secs on, 60 secs off in the bare resonator condition. Fig.3-13 shows a plot of the output energy -vs- number of shots at 1pps. The output repeated in the second and third "on" periods at slightly lower output levels.

Output variation due to rod bending and resonator misalignment had been anticipated in the single flashlamp cavity, however, the large variation in output energy over 1 cycle in long pulse operation prompted an examination of rod stability.

Three potential mechanisms exist for generating rod movement. The first is motion of the sapphire tube caused by TE cooler movement. The second is non-uniform absorption of the flashlamp pump energy creating a thermal gradient and causing the rod to bend independently of the sapphire tube. The third possibility is O-ring motion caused by absorption of the flash-lamp pump energy.

To isolate these effects a mirror was bonded to the hot side of the sapphire tube and the rod probed with a HeNe laser through a 1 meter lens. Little or no motion of the reflected spot was detected under 10x magnification when the TE cooler was operated at 1 amp and the flashlamp pumped at design duty cycle and rep rate (E in = 24 joules). The mirror was removed and both ends of the laser rod probed with the HeNe.

Figure 3-13

Long Pulse Output (bare resonator condition)
and Front Face Rod Deflection -vs- Number of
Shots.
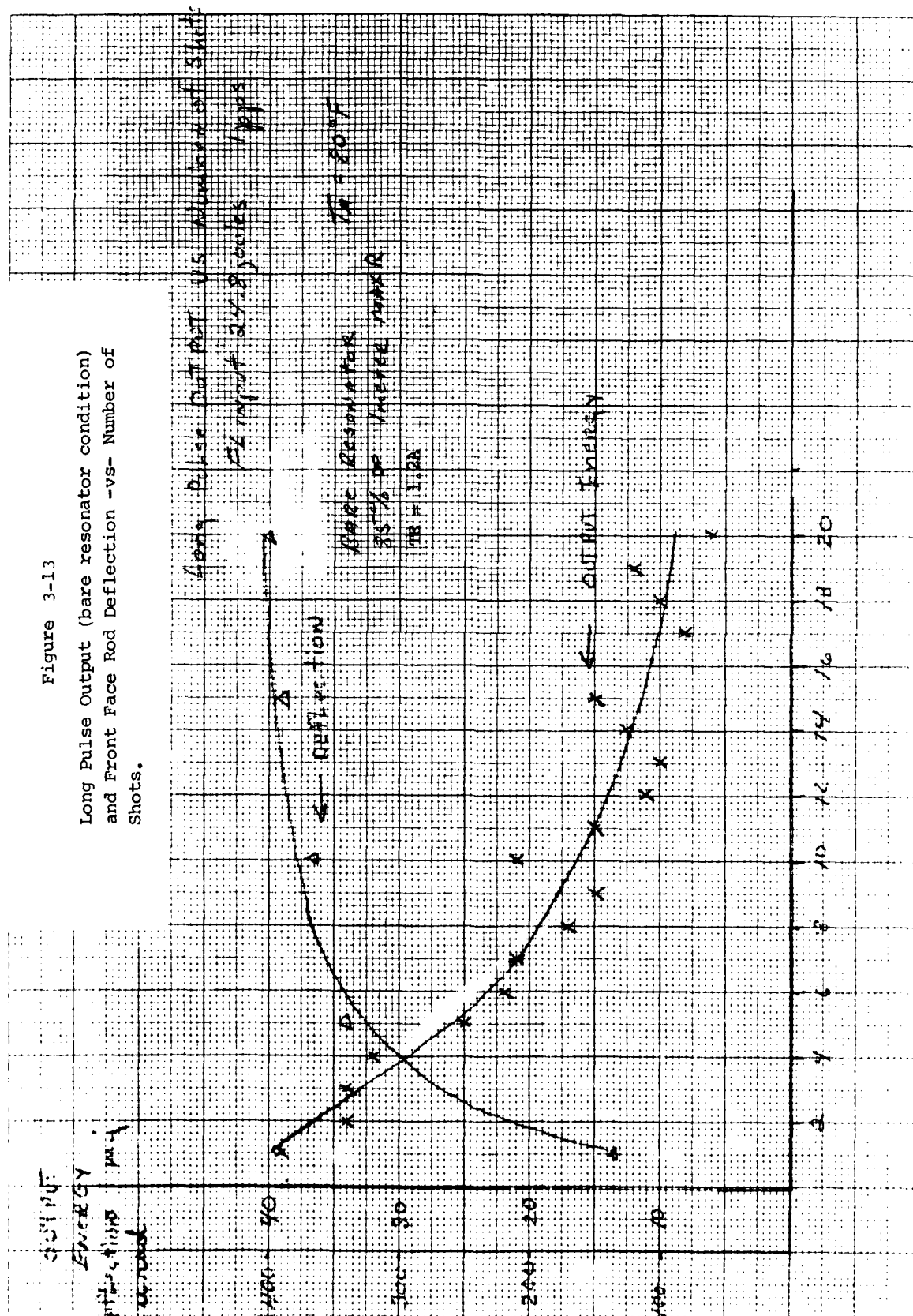
The cool side face deflected away from the flashlamp by as much as 400 urad at the end of the first 20 secs "on" period. Movement appeared to be entirely in the vertical plane and recovery was essentially complete at the beginning of the second "on" period. A plot of front face rod deflection versus number of shots is shown in Figure 3-13. The hot side face deflected with similar characteristics 130 urad away from the flashlamp.

The rod was examined for O-ring induced motion by shielding the outside of the sapphire tube in the vicinity of the O-rings with aluminum foil, thereby inhibiting absorption of flashlamp radiation by the O-rings. The cool side face was again probed with the HeNe and the flashlamp operated at 1 pps 20 secs on, 60 secs off (TE = 1 amp). The maximum deflection was 380 urad - not significantly different from the previous tests.

Figure 3-13 demonstrates a correlation between thermal gradient induced rod deflection and laser output. However, wavefront distortion, bulk heating of the rod, and thermal focussing remain potential factors effecting laser output.

2) Q-SWITCHED OPERATION

Single pulse Q-switched operation is a key factor in obtaining satisfactory rangefinder performance from Ho:YLF. We have earlier in this section detailed the significant problems encountered in obtaining this type of operation. Briefly restated, they are:

- Slow resonant transfer times between sensitizing ions and holmium ions resulting in long energy storage times and multiple pulsing.

- Residual retardation induced by the $LiNbO_3$ creating high cavity losses even though voltage across the crystal is zero.

- Piezoelectric ringing in $LiNbO_3$ causing oscillations in the retardation induced by the crystal and subsequent multiple pulsing.

Limiting Q-switched outputs to a single pulse has given rise to a square wave Pockel's Cell Q-switch that is positively switched to an off-state once laser output is obtained and prior to any after-pulses. Work performed under an RCA IR&D program dealing with crystal mounting techniques has resulted in reduced piezoelectric ringing.

a) Square Wave Switch

The net switching voltage waveforms applied to the $LiNbO_3$ crystal have been detailed in Section III B. A schematic of the high voltage switch is shown in Figure 3-10.   An optional 500 Ω resistor R_A could be placed in series with the $LiNbO_3$ to vary the rise time of the high voltage waveform applied to the crystal. V_{BB} was a high voltage power supply controlling the Pockel's Cell hold off voltage. Width of the HV pulse and therefore the Pockel's cell "on" time could be varied by adjustment of the RC timing network indicated on the schematic. On times of less than 1 usec to 100 usecs were possible. Figure 3-14 shows the voltage waveform across the $LiNbO_3$ crystal. Rise time with and without the 500 Ω series resistor was 700 ns and 50 ns respectively.
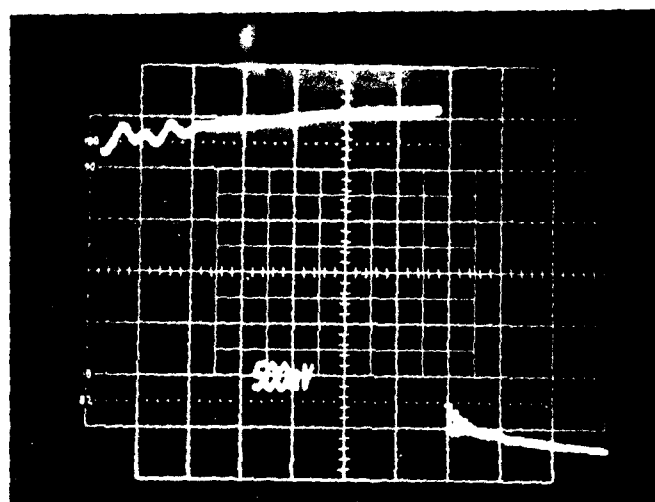
3-25

Figure 3-14

High Voltage Waveform across LiNbO$_3$

Pockel's Cell. (500V/div, 1 usec/div, RA=0)

b)   Single Pulse Q-Switched Output

Single pulse Q-switched operation was obtained with the same resonator as that used in the previous pulse tests.   The LiNbO$_3$ crystal was 5x5x15 mm and AR coated at 2.06 um.   Mirrors consisted of an 85% flat and 1 Meter MAXR.   Resonator length was approximately 9 inches.

The Pockel's cell polarizer was a zinc selenide (ZnSe) flat oriented at Brewsters angle.   ZnSe was selected because of its high refractive index (n = 2.44) allowing a maximum theoretical polarization loss of 50% per surface.   In addition ZnSe is transmissive in the visible thereby aiding resonator alignment.   Insertion loss of the Pockel's cell components is given in Table 3-4.

Typical long pulse output energies for the fully assembled resonator were 33-38 mj (24.3 joules, TE = .6A, T_A = 80°F, 3-4ppm).   Figure 3-15 is a photo-graph of the long pulse output detected by the InAs detector.

The best Pockel's Cell (PC) hold-off occurred when V_{BB} was adjusted to 2900-3000V.   No output was detected with the InAs Detector at this hold off voltage.   The PC high voltage switch was then adjusted to approximately 3000V thereby leaving a residual bias of less than 100V on the crystal during switching.   Based on previous experience with Ho:YLF the Q-switching took place 400-500 usec after the flashlamp trigger.   Q-Switch on time was 10 usecs.   Single pulse outputs were repeatably and reliably maintained at 3-4ppm as shown in Figure 3-16.   Optical pulse width was 100-180 ns FWHM.   Output energy remained low - approximately 4-5 mj per pulse.   Q-Switched output could be obtained for PC delays of 300 to 700 usecs.   No difference in output characteristics was observed in varying the rise time of the PC high voltage switch between 50 and 750 nsecs.
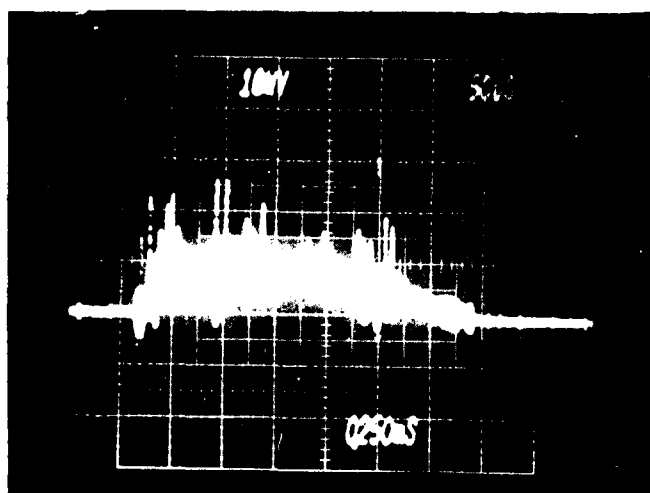
Figure 3-15

Long Pulse Output of Q-Switched Resonator.

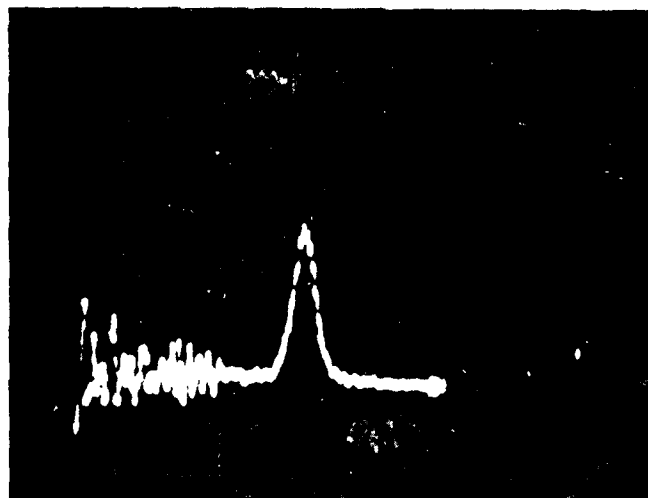(50 usec/div, 10mV/div, Scope delay = 250 usecs, 85% ∞ , 1 meter MAXR)

Figure 3-16

Trace of Attenuated Laser Output
showing FWHM ≈ 100ns (200mV/div,
200 ns/div, Scope delay = 427 usecs).

The effect of increased PC ON time is demonstrated in Figure 3-17 in which is shown the added oscilloscope trace of the InAs detector and high voltage switching waveform across the PC. A single pulse is obtained during a 10 usec on time with laser output beginning approximately 500 ns from the start of the HV switch.

Figure 3-18 shows a 33 usec PC in time in which the primary Q-switched output (saturating the InAs detector at 4V) occurs immediately after PC turn-on and is followed by three weaker afterpulses as much as 32 usec later. Though single pulse output energies remained in the 4-5mj range, suppression of afterpulsing and attainment of reliable single pulse operation using square wave switching is a significant step in obtaining PC compatibility with Ho:YLF.

c)   Beam Divergence (LiNbO$_3$ Q-Switch)

Beam divergence of the Q-switched laser was measured by firing the laser through a lens whose 2.06 um focal length is 62.4 inches and measuring the energy transmitted through various apertures in the focal plane. The laser was operated 3-4 ppm with a TE cooler input of .6A and a flashlamp pump energy of 24 joules. Figure 3-19 is a plot showing the percentage of the total output energy transmitted by an angular aperture given by the abscissa. Approximately 80% of the total energy was received within a 2.8 mr aperture.

d)   1pps Q-Switched Operation

After performing the low rep rate beam divergence tests the laser was operated Q-switched at the 1pps, 20 secs on, 60 secs off design goal. Typically Q-switched output ceased after 10-15 shots in the first 20 secs on period and after 10-12 shots in the second period for constant energy input and single ended TE cooling Figure 3-20 shows a plot of output energy versus number of shots for a single cycle. Pertinent operating parameters are given in the figure.
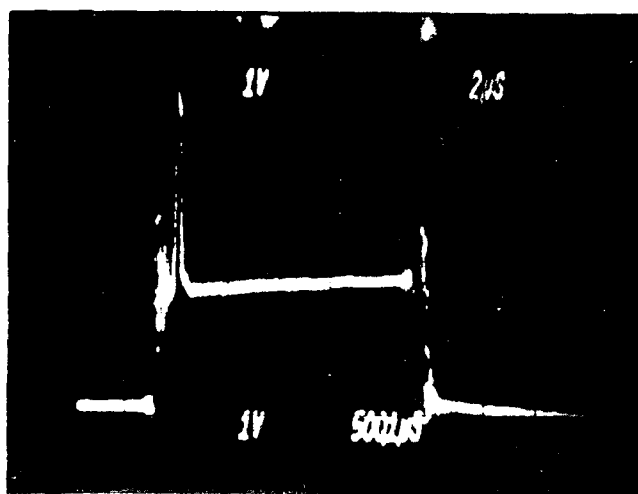
Figure 3-17

Added trace of InAs detector and Output
of Pockel's Cell pulse circuit. (2 usec/div,
1000V and 1v/div 500 usecs scope delay).
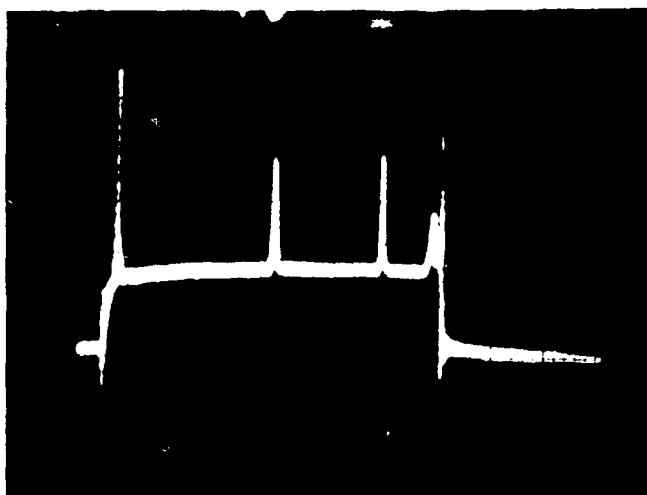Output energy ≈ 5mj. Ein = 24 joules.

Figure 3-18

Multiple pulsing due to increased PC on
time (33 usec). (2000V/div 1v/div, 5 usec/div,
scope delay = 463 usec) Added trace of InAs de-
tector and HV on PC.

Figure 3-19

Beam Divergence of Low Rep Rate
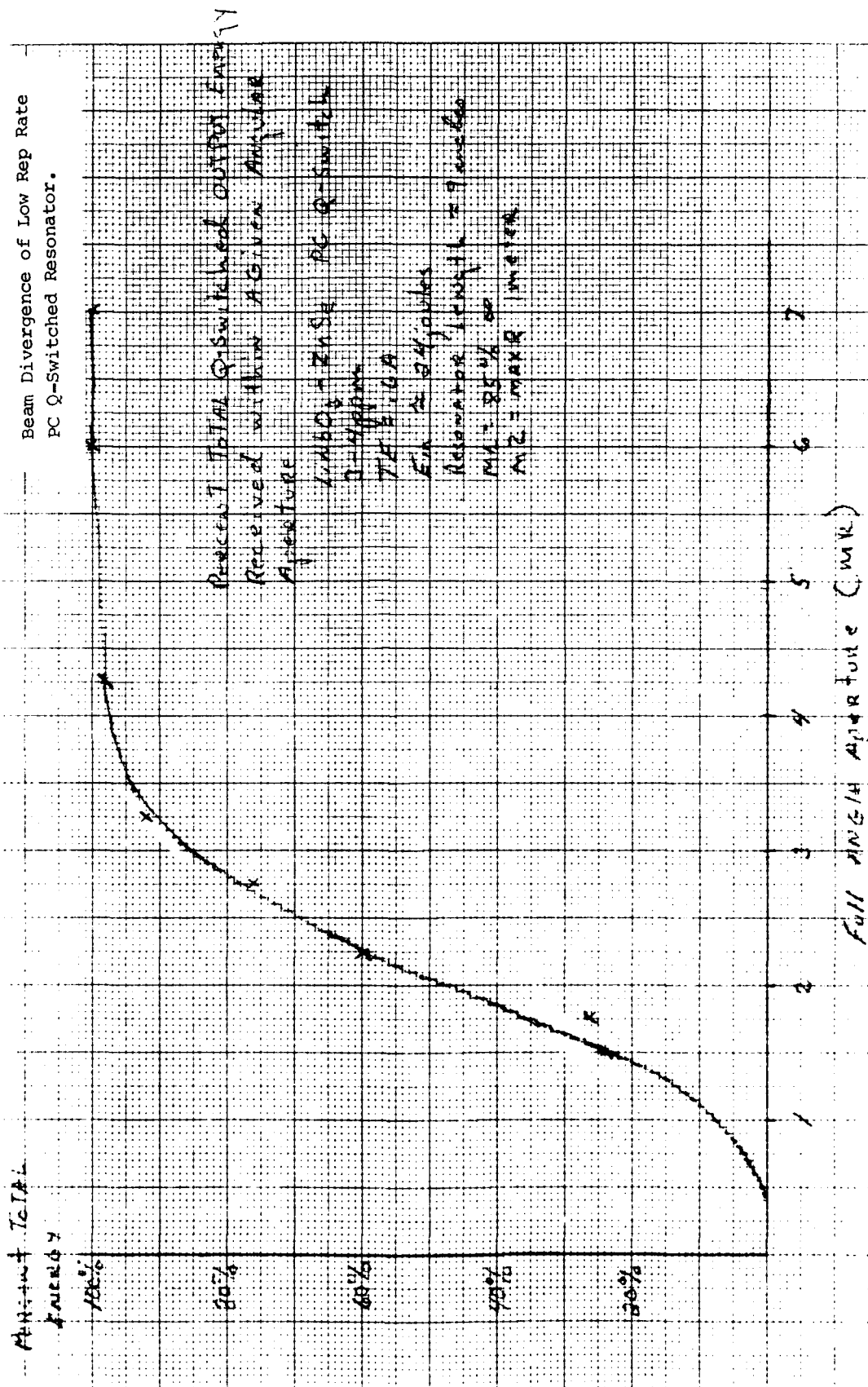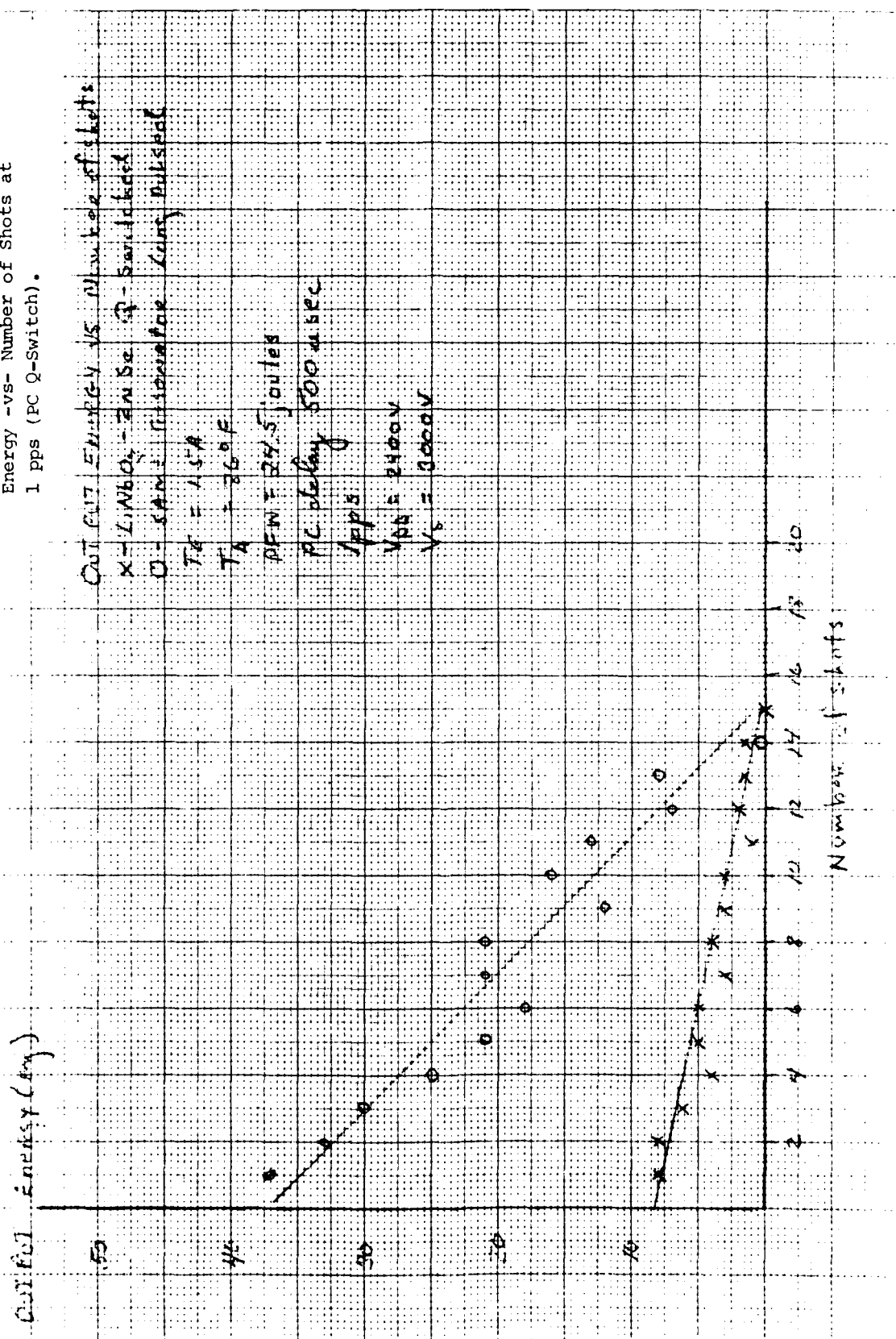PC Q-Switched Resonator.

Figure 3-20

Long Pulse and Q-switched Output
Energy -vs- Number of Shots at
1 pps (PC Q-Switch).

Initial Q-switched output energies of 8 mj declined to 0 mj in 15 shots. This was typical of several runs. Also shown in Figure 3-20 is the output energy versus number of shots of the laser when operated long pulse. Long pulse output could be maintained for as long as 19 shots, however, the run shown is typical. Long pulse to Q-switched output energy conversion efficiency was 20-25% throughout the run. Applying switching back-biases of as much as 1100 Volts to eliminate any residual retardation did not substantially alter the conversion efficiency. This would seem to indicate a residual retardation persisting in the $LiNbO_3$ crystal during the PC on time was not responsible for the low conversion factor since back-biasing the crystal allows any residual retardation to be nulled out. The low conversion ratio may in part be due to small amount of piezoelectric ringing which prematurely terminates the Q-switched pulse by varying PC transmission away from maximum. Figure 3-20 also indicates that if long pulse energy were maintained at its initial levels, e.g. by increasing pump energy, there is no fundamental Q-switch problem in obtaining 8-10 mj PC Q-Switched outputs.

Fig. 3-21 shows multiple traces of the added InAs detector and HV switching waveform across the PC. Each trace results from a single firing of the laser and is stored and simultaneously displayed with previous firings on the oscilloscope thereby allowing the pulse timing characteristics of two or more shots to be compared. Each firing of the laser resulted in only one of the output pulses seen in the photograph. Pulse width information should not be inferred from these photographs since the InAs detector was allowed to saturate to enable any small afterpulses to be readily observed.

The top photograph of Fig. 3-21 shows the first five pulses of a thirteen pulse series at 1pps. Each pulse occurs repeatably with respect to the start of the HV switch. Variations in pulse position seen in the photograph are due to 500 ns jitter in the PC delay time. The lower photograph shows the last 5 pulses of the series. The amplitude of these pulses is decreasing, however, single pulse operation was maintainted throughout.

Figure   3-21

Added trace of InAs Detector and PC Voltage
showing Multiple Laser Firings (1 usec/div,
1000V and 1v/div, TE=1.3A, scope delay = 500 usecs.)
Top photograph of first 5 pulses of 13 pulse series.
Bottom photograph of last 5 pulses of 13 pulse series.
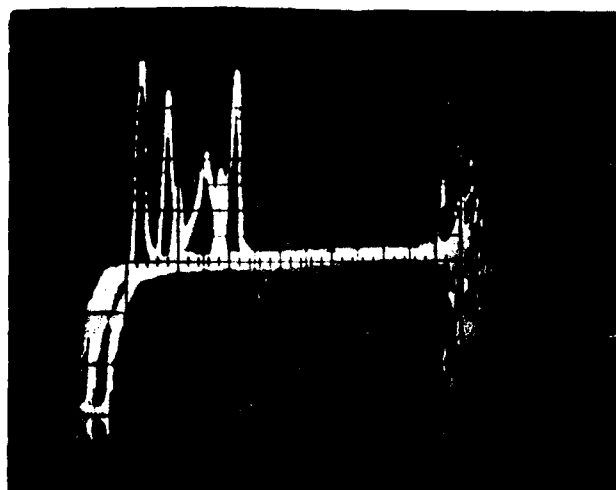
The pulse buildup time has increased substantially, usually an indication of higher threshold operation. Attempts at maintaining high output energy by dynamically aligning the resonator at 1 pps were unsuccessful.

e) High Gain Q-Switched Output

Standard procedure in maximizing output energy and obtaining desirable laser pulse shapes using Pockel's Cell Q-switches is rotation and alignment variation of the retarding crystal. In evaluating the Q-switched output of Ho:YLF the $LiNbO_3$ crystal was rotated and realigned relative to the ZnSe polarizer several times. In one orientation long pulse output energies of 60-70 mj (24 joule pump, PC delay 500 usec, TE = .7A) were obtained. This represented a 50%+ improvement over the 40 mj obtained in several other orientations and already described in this report. Long pulse outputs of 60-70 mj could lead to substantially higher Q-switched output energy when operating at 1pps.

V_{BB} was varied from 1000 to 4000 volts to determine the optical hold off condition. Incomplete hold off could be obtained for V_{BB} = 2900-3100 volts, however, 4-5 spikes occurred 400-500 usec after the flashlamp trigger. Ultimately hold off could only be obtained by reducing the electrical input energy to the flashlamp to less than 23 joules.

Fig. 3-22 demonstrates the effects of insufficient hold off. Despite a large single pulse during the PC on time, pre-lasing takes place 10 usec prior to switching and after pulsing 30 usecs after the HV switching.

Single pulse Q-switched outputs (8 mj per pulse) were ultimately obtained (PC delay 500 usec, E in = 23 joules, TE = .7A) by operating at a constant 4 ppm rep rate and precise adjustment of V_{BB} (=2930 volts) relative to the PC switching voltage of 3400 Volts (net back bias 470 Volts).
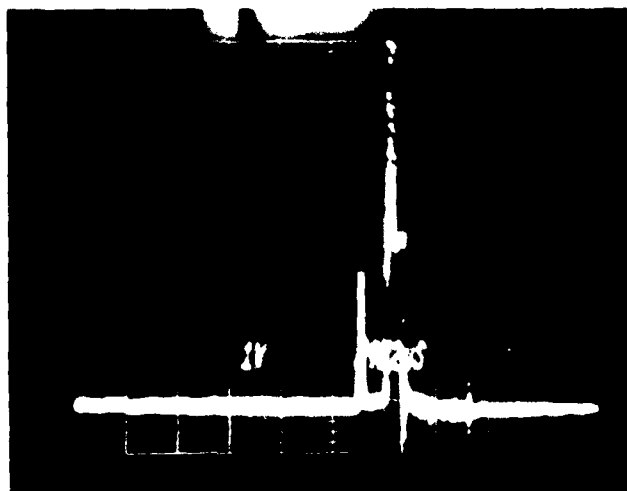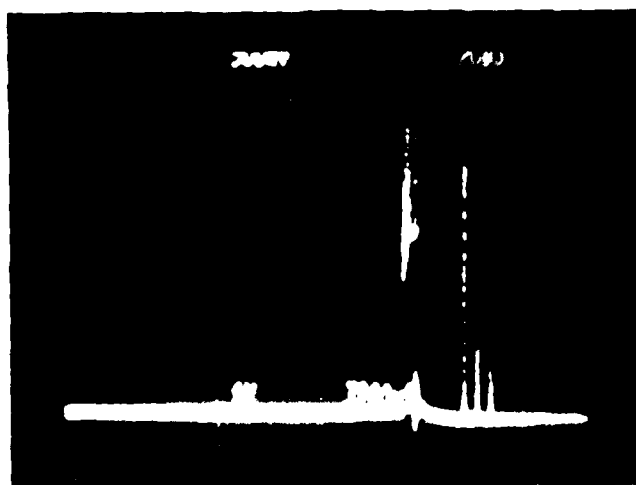
Figure   3-22

Pre-lase and after pulsing of Square Wave
Q-switched Ho:YLF. Added trace of InAs
Detector and PC high voltage (1000 V/div
.5v/div, 20 usec/div. 85% flat 1 meter
MAXR, Ein = 24 joules.)

The constant rep rate requirement is not unexpected due to Ho:YLF's threshold sensitivity to temperature. Variation of the rep rate will effect the rod temperature and threshold, laser output, and therefore, the PC holdoff required.

It is estimated that neglecting resonator losses other than the 85% output mirror and the Pockel's Cell, a loss of 94% per pass must be induced by the Pockel's Cell for hold off of a 60 mj pulse. Since the maximum loss induced by the ZnSe polarizer (n = 2.44) per pass is 25%, a single ZnSe Brewster angle polarizer will not prevent lasing with a population inversion sufficient to generate a 60 mj long pulse output. A second ZnSe Brewster angle polarizer would be necessary to generate the required losses.

f) ROTATING MIRROR Q-SWITCH

Program time constraints did not permit additional optimization of the LiNbO3 Pockel's Cell Q-Switching. However, in an internal RCA program a rotating mirror Q-Switch was substituted for the Pockels Cell and the feasibility of TE cooling in providing 1 pps operation of Ho:YLF demonstrated in tests up to 140°F. A double ended TE cooling arrangement was also incorporated for additional cooling capacity. The results of these tests are presented for completeness. Our previous experience with rotating mirror Q-Switches has shown them capable of providing single pulse outputs and 60-80% long pulse to Q-switched energy conversion efficiency. There is a further advantage in that eliminating the Pockel's Cell typically reduces threshold and shortens the resonator.

The rotating mirror resonator consisted of a 85% ∞ output mirror and 1 meter MAXR mounted in the rotor of the Q-Switch. Overall resonator length was reduced to 6.5 inches mirror-to-mirror.

Single pulse output energy was approximately 14 mj or nearly 50% higher than outputs obtained using the Pockel's Cell under the same operating conditions. Higher pulse energies are attributed to lower threshold and resonator losses. Q-Switched threshold was 18.2 joules. The beam divergence was measured as previously at 3-4 ppm and is shown plotted in Figure 3-23. Eighty percent of the total output energy was contained within a 3.75 mr aperture.

Initial output energy levels of 40-50 mJ at 25 J input with maximum cooling during the first several shots resulted in three bulk damage sites. The most serious site is shown under 30x magnification in Figure 3-24. Peak power in the resonator was estimated to be $300MW/cm^2$.

Figure 3-25 shows the output pulse shape as detected by the InAs detector. FWHM of the single pulse output is 55 ns.

Sustained operation was the result of observing the laser output and manually varying the flashlamp pump energy to maintain the output energy at 9-12 mJ. In practice, this type of operation could be easily obtained by thermistor temperature sensing and a programmable power supply. The unit was successfully operated at this energy level and duty cycle up to $140^{\circ}F$.

Threshold of the first pulse in each cycle increased through the third cycle and was nearly constant thereafter. Figure 3-26 dramatically illustrates the desirability of TE cooling of Ho:YLF. Shown are flashlamp pump level requirements at the beginning and end of the fourth or fifth cycle at each ambient temperature. Pump level swings are fairly small (6 joules) at room temperature. However, as the limit of TE cooling capacity is reached higher initial pump levels are required. Higher pump energies increase the rod heat load and operating temperature, and create a need for ever increasing pump levels at the end of each cycle. This continued until ultimately 50 joules and a pump level swing of 17 joules is required for the last cycle at $140^{\circ}F$.
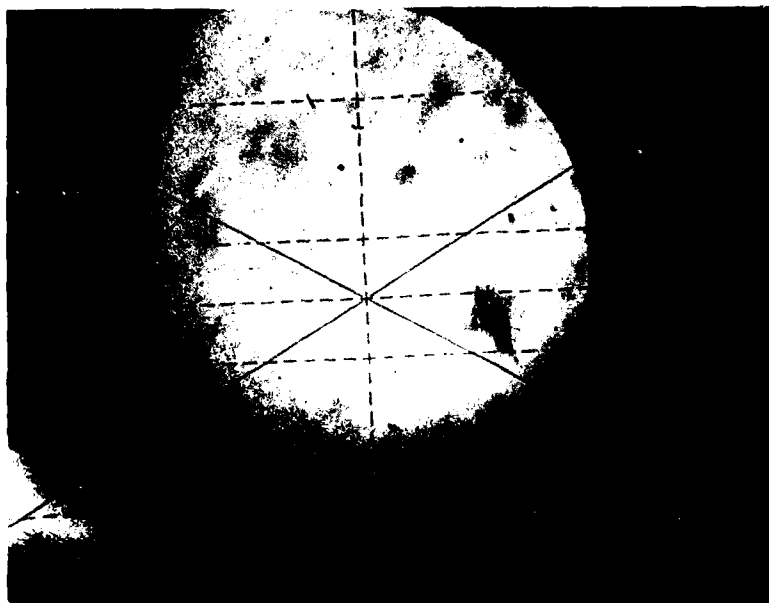
Figure 3-23

Beam Divergence Rotating Mirror Q-Switch.
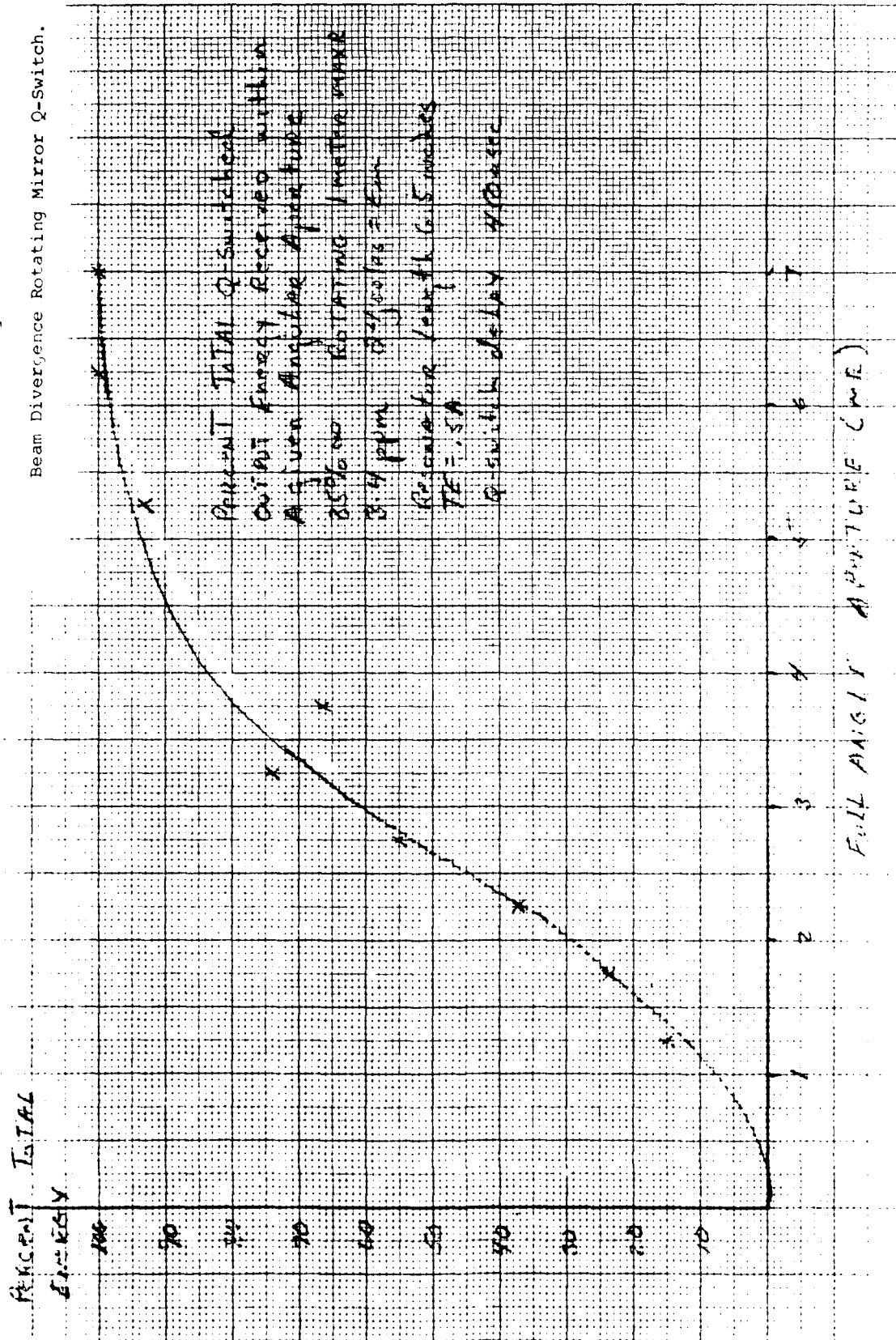
Figure 3-24

Largest bulk damage site of three observed
after Q-switching (rotating mirror) over
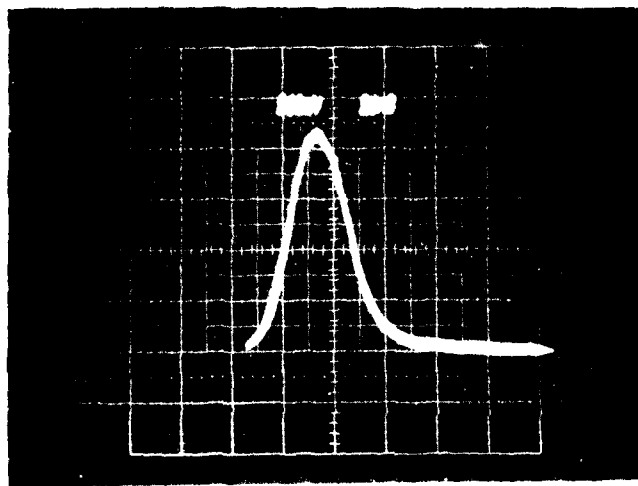30mj (50ns FWHM), 85% R). φ Magnified 30x.

Figure 3-25

Output pulse (InAs detector into 50 Ω)
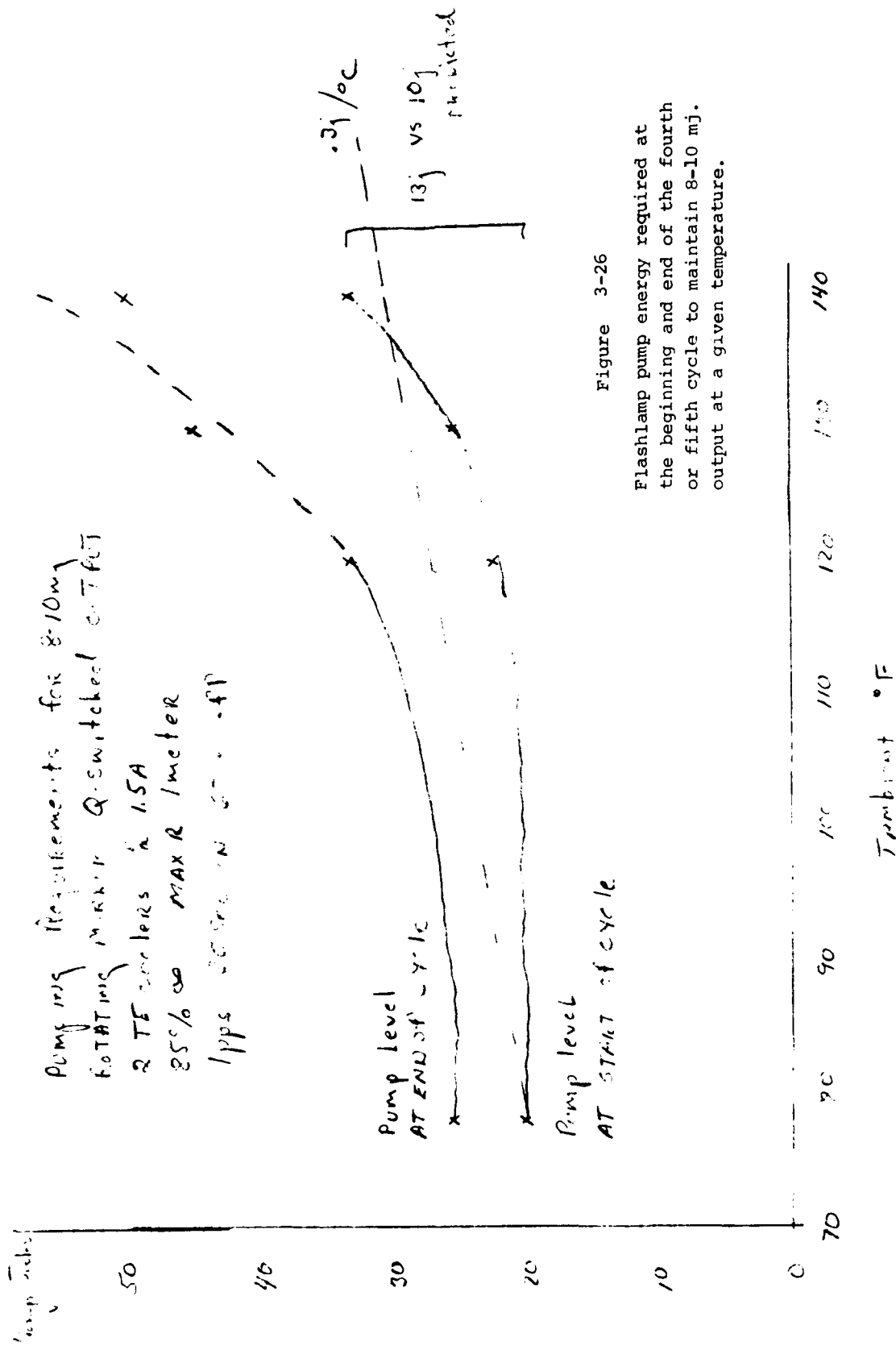showing 55ns FWHM.

Figure 3-26

Flashlamp pump energy required at the beginning and end of the fourth or fifth cycle to maintain 8-10 mj. output at a given temperature.

IV

CONCLUSIONS AND RECOMMENDATIONS

This program has demonstrated that the Ho:YLF laser in conjunction with a thermoelectrically cooled HgCdTe detector receiver makes practical a small laser rangefinder (LRF) operating at 2.06 micron with currently available technology. Repetition rates of up to 1 pps are possible from Ho:YLF laser over military temperature ranges using simple compact, thermoelectric cooling of the Ho:YLF laser rod. Such a laser rangefinder can utilize many of the components developed for Nd:YAG laser rangefinders. This has been demonstrated by quantitative ranging experiments, and laboratory tests. The ranging tests have demonstrated conclusively that atmospheric CO_2 absorption of the 2.06 micron attenuation to meterological visibility in kilometers) of 3.0 - 3.5 can be utilized to predict performance. In summary, this program has demonstrated the technological practicality of a 2.06 micron LRF for military applications where this wavelength is attractive for eye-safety or smoke penetration reasons. The LRF has been certified eye safe at the exit aperture (11).

The sensitivity of the rangefinder receiver could be improved significantly (by a factor of three to four) by optimizing the HgCdTe detector material for peak response at 2.1 micron instead of the 3.7 micron peak response material utilized. Frequency boosted preamplifiers can be utilized with present photoconductive HgCdTe detectors to achieve adequate overall bandwidth for rangefinder applications since the preamplifier is at present not the noise limiting element of the receivers. Additional improvements in rangefinder performance can be achieved with greater laser output energies than the ~ 5-10 millijoules utilized on this program. A 20 millijoule laser in conjunction with an optimized 2.0 micron HgCdTe detector should yield a rangefinder with a 3 km range capability with 3 km visibility against a 10% reflectivity target which is quite comparable to present Nd:YAG/Silicon Avalanche detector rangefinders with comparable physical sizes and weights. Transmission measurements at 2.06 micron should be performed for typical battlefield

obscurants such as smoke. This assumes that a satisfactory optical and coating design is achieved which can combine the visual sighting and receiving functions with good transmission and resolution at both visible and 2.06 micron wavelengths. Many currently utilized glasses and coatings for the visible have high losses at 2.06 micron.

In view of the above, continued development is indicated in several areas. Further HgCdTe material development and evaluation should be pursued to achieve 2.1 micron peak response with a NEP of 1×10^{-12} watts/$\sqrt{Hz}$ with adequate frequency response using either photoconductive HgCdTe with boosted preamplifiers or photovoltaic HgCdTe. An optical design study is necessary to determine the feasibility of combining the visual sighting and 2.06 micron receiving functions for typical military rangefinder applications. In addition some additional engineering development of miniature Q-switched Ho:YLF lasers with 1 pps repetition rates capability with 20 millijoule output and non-rotating mirror Q-switches is indicated, although the basic performance and techniques have been demonstrated.

REFERENCES

1. E. Schiel, V. Rosati, R. Buser, E. Chicklis, C. Naiman, R. Folweiler, "Two Micrometer Laser Rangefinder and Target Resignator (U)" Proceedings of the Sixth DOD Conference on Laser Technology, Vol. II, March 1974, p. 453.

2. K. White, W. Watkins, S. Schleusner, "Holmium 2.06 um Laser Spectral Characteristics and Absorption by CO_2 Gas", Applied Optics, Vol. 14, No. 1, Jan. 1975, p. 16.

3. M. B. Reine and R. M. Broudy, "A Review of HgCdTe Infrared Detector Technology", SPIE Vol. 124 Modern Utilization of Infrared Technology III (1977), p. 80.

4. T. Tredwell, "HgCdTe Photodiodes for Detection of Two Micrometer Infrared Radiation", Optical Engineering, Vol. 16, No. 3, May 1977, p. 237.

5. Target Signature Analysis Center: Data Computation, University of Michigan, July 1969.

6. L. Elterman, "Vertical Attenuation Model with Eight Surface Meterological Ranges 2 to 13 Kilometers", Report AFCRL-70-0200.

7. "Development of Multipy Sensitized Ho:YLF as a Laser Material", E. P. Chicklis, et al, ECOM Technical Report ECOM-78-0066-F.

8. "Transient Elastooptic Effects and Q-Switching Performance in $LiNbO_3$, and KD*P Pockels Cells", R. P. Hilberg and W. R. Hook, Applied Optics, August 1970.

9. "Optical Pumps for Lasers", L. Noble, et al. ECOM Research and Development Technical Report ECOM-0239-F, October 1973.

10. "Optical Pump for Holmium Lasers", L. Noble, et al, ECOM Research and Development Report ECOM-72-0274-F, July 1974.

11. "Non-ionizing Radiation Protection Special Study No. 25-42-0300-79 Holmium Laser Rangefinder", U.S. Army Environmental Hygiene Agency, Aberdeen Proving Ground.